16

High-Power Pulsed 2-μm Tm^{3+}-Doped Fiber Laser

Yulong Tang and Jianqiu Xu
Key Laboratory for Laser Plasmas (Ministry of Education) and Department of Physics, Shanghai Jiao Tong University, Shanghai, China

1. Introduction

1.1 Research background

Laser beam in the 2~3μm spectral range has wide applications. It is a good candidate in laser microsurgery due to high absorption of water in this spectral region. It can also be used in environment monitoring, LIDAR, as optical-parametric-oscillation (OPO) pump sources, and so on [1-4].

Tm^{3+}-doped fiber is very suitable for producing ~2-μm laser emission due to its several unique advantages. First, Tm^{3+}-doped fiber has a strong absorption spectrum that has good overlap with the emission spectrum of commercially available AlGaAs laser diodes. Second, the specific energy-level structure of Tm^{3+} ions provides the Tm^{3+}-doped fiber laser (TDFL) quantum efficiency close to two through the cross relaxation (CR) process. Thirdly, the Tm^{3+}-doped fiber has a very broad emission band (~400 nm), offering great wavelength tunability for the fiber laser.

For achieving high-power output, Tm^{3+} ions are often doped into silica glass fiber to construct 2-μm fiber lasers. The silicate glass fiber has maximum phonon energy as large as 1100 cm^{-1} (compared to 550 cm^{-1} for fluorides) [5], which limits its infrared transparency wavelength less than 2.2 μm.

In the past, the fiber laser was usually core pumped. Small fiber core area (<100 μm^2) requires high brightness of the pump beam, greatly limiting the pump power than can be launched into the fiber core. With the advent of double-clad fiber configuration, the pumping area was changed to the cladding area (>10000 μm^2), significantly facilitating pump-power launching. From then on, the output power of fiber lasers has been greatly enhanced.

For fiber laser oscillation, the simplest (commonly adopted) laser resonator is defined as Fabry-Perot resonator, which is shown in Fig. 1. The pump light is launched into the fiber through a dichroic mirror, high transmissive for pump beam but high reflective for laser light. Laser oscillation forms between this dichroic mirror and the distal-end fiber facet (~4% Fresnel reflection).

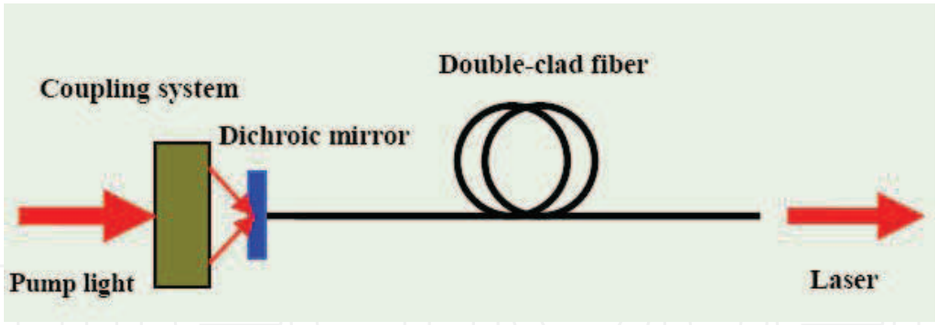

Fig. 1. The Fabry-Perot Tm^{3+}-doped fiber laser resonator.

The simplified energy-level diagram of Tm^{3+} ions is shown in Fig. 2. The pump light at ~790 nm excites Tm^{3+} ions from $^3H_6$ to $^3H_4$, which then nonradiatively decay to the upper laser level of $^3F_4$ with a fluorescence lifetime of 0.55 ms [6]. The transition from $^3F_4 \rightarrow {}^3H_6$ will radiate photons at wavelength of ~2 μm. Due to large Stark splitting of the energy levels, the TDFL is a quasi-four-level system.

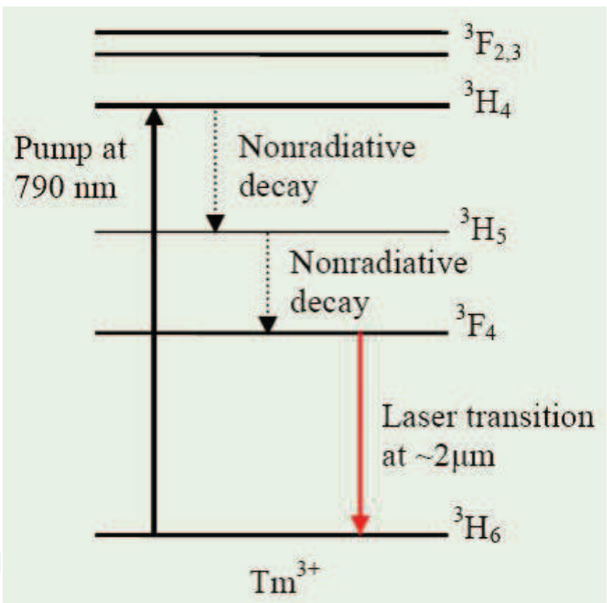

Fig. 2. The simplified energy-level diagram of Tm^{3+} ions.

The Tm^{3+} ion has fluent energy levels, providing complex energy-transfer processes. The **CR** process ($^3H_4+{}^3H_6 \rightarrow {}^3F_4+{}^3F_4$), as shown in Fig 3, is very beneficial for improving slope efficiency of the TDFL. With the help of this process, high quantum-efficiency TDFLs have been realized [7-8], and the slope efficiency has surpassed 60% [9-10].

For high-power ~2μm TDFLs, 790-nm AlGaAs diode lasers are preferred pump sources. This pump wavelength is the only appropriate wavelength to stimulate the beneficial CR process for TDFLs. Aside from 790 nm, laser sources at other wavelengths can also be used as the pump source, including Nd:YAG lasers (1.064 and 1.319 μm), Yb-doped fiber lasers (1.09 μm), Er^{3+}-doped fiber lasers (1.57μm), and so on.

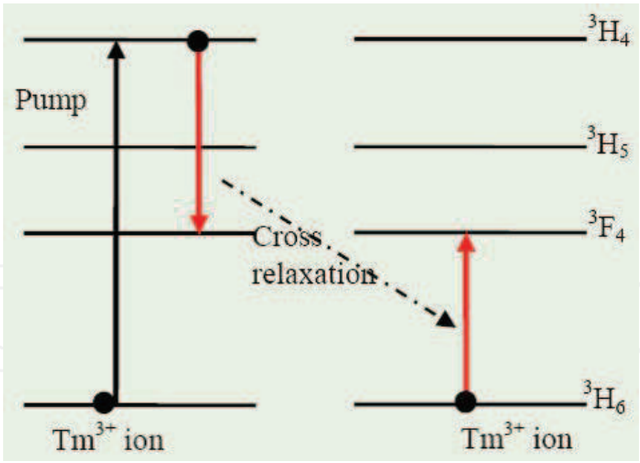

Fig. 3. Cross relaxation between Tm^{3+} ions.

1.2 Recent development of Tm^{3+}-doped fiber laser

The first ~2μm TDFL was achieved by Hanna et al. in 1988 with a 797-nm dye laser as the pump source [11]. With the advent of AlGaAs diode lasers as the pump source, the all-solid-state Tm^{3+}-doped silica [12] and fluoride [13] fiber lasers were both realized in 1990.

High-power TDFLs had not been achieved until the invention of double-clad pumping configuration by Snitzer et al. in 1989. The first high-power TDFL was reported by Jackson in 1998, with maximum output of 5.4 W and slope efficiency of 31% [14]. In 2000, Hanna et al. [15] improved the output power of the TDFL to 14 W with a slope efficiency of 46%. In 2002, the 2-μm TDFL has achieved an output power of 85 W by Jackson et al. [16], the slope efficiency being 56%. At nearly the same time, 75 W 2-μm laser output was also realized in an Yb-Tm codoped fiber laser [17], where Yb3+ ions were used as sensitizers to facilitate pumping with 976-nm diodes. However, the slope efficiency was just 32% due to the lack of the "cross relaxation" process. In 2007, G. Frith reported a TDFL with output power of 263 W and slope efficiency of 59% [18]. In 2009, the 2 μm output power from the TDFL was significantly enhanced to 885W with a slope efficiency of 49.2% [19], and exceeded one kilowatt [20] just one year later. At present, single frequency output has also been over 600 watts [21]. These significant developments in 2-μm TDFLs have made them a much attractive tool in many application areas.

Along with the power scaling of continuous-wave (CW) TDFLs, many works have also been carried out to realize high-peak-power or short-pulse-duration TDFLs. The first 2-μm Q-switched TDFL was carried out in 1993 with an acousto-optic (AO) modulator [22]. The pulse width was 130 ns, and the peak power was only 4 W. In 1995, 2-μm femtosecond (500 fs) laser pulse was first achieved in Tm fiber [23]. By also using AO modulator, a peak power of 4 kW (with pulse width of 150ns) TDFL was realized in 2003 [24], but the average power was just 60 mW. In 2005, by adopting an amplification configuration, the peak power of 2μm Tm fiber laser has reached 230 kW (108 fs) with improved average power to 3.1 W [25]. For achieving high pulse energy from TDFLs, the gain-switching technique is usually employed. In 2000, 2-μm TDFL has achieved 10.1-mJ pulse energy [26], which was further improved to 14.7 mJ in 2005 [27]. These gain-switching TDFLs were often accompanied by

relaxation spikes, showing comparatively low system stability. Recently, special measures (such as employing high pump ratio or combined gain-switching and amplification) have been applied to scale the averaged 2-μm pulsed laser power to tens of and even hundred watt levels [28–32].

2. High power acousto-optic Q-switching Tm^{3+}-doped fiber laser

Nowadays, high-average-power 2-μm pulsed laser are eagerly required in pumping 3~4-μm mid-infrared lasers [33], environmental detecting [34], and medical surgery. For 2-μm TDFLs, pulsed operation can be realized through either Q-switching or mode-locking. Q-switching can usually provide a somewhat higher average power, but mode-locking operation can often provide much narrower pulse width thus higher pulse peak power. In this section, we mainly introduce AO Q-switching operation of TDFLs for achieving high-power 2-μm laser pulses in our laboratory.

2.1 Power scalability of pulsed Tm^{3+}-doped fiber laser

In our experiment, the double-clad Tm^{3+} silica fibers have a Tm^{3+} concentration of ~2wt.%. The fiber core has a diameter of ~30-μm and a numerical aperture (NA) of 0.09. The pure-silica inner cladding is D-shape, and has a 400-μm diameter and a NA of 0.46. The absorption coefficient of the fiber at the pump wavelength (~793 nm) is about 3 dB/m.

The experimental setup for the AO Q-switched TDFL is shown in Fig. 4. The pump source was a pig-tailed high-power laser diode (LD) operated at 793 nm with a total output power of ~110 W. The pig-tail fiber has a diameter of 200 μm and an NA of 0.22. Two aspheric lenses were used to couple the pump light into the fiber, with a coupling efficiency of ~90%. A dichroic mirror (T=97%@793nm&R=99.5%@2μm at 45° coating) was employed to transmit the pump light and extract the 2-μm laser beam. A high-reflection mirror (R=99.5%@2000nm) at the far end is used to provide the laser light feedback, which together with the perpendicularly cleaved pump-end fiber facet (~3.55% Fresnel reflection for laser oscillation) complete the laser cavity. The Tm^{3+}-doped gain fiber is wrapped on a copper drum or immerged in water for cooling. At both fiber ends, a short piece of gain fiber (with the polymer coating removed) is placed between a copper heat sink for efficient heat cooling. At the output end of the fiber, another dichroic (T=98%@2μm&R=99.8%@793nm) is used to filter the residual 793-nm pump power. The AO Q switch is inserted between the far fiber end and the high-reflection mirror. The far end fiber is angle-cleaved (~8°) to avoid the parasitic oscillation due to fiber-facet reflection. The laser output power was measured with a thermal power meter and the laser spectrum was tested with a spectrometer.

Figure 5 shows the average output power of the *Q*-switched TDFL with respect to the 793-nm launched pump power at the repetition rate (RR) of 50 kHz. The maximum laser power was ~32 W with a slope efficiency of 36%. At high power level, the AO switch could not switch off completely, leading to decreased signal-to-noise ratios. This is an important issue that should be addressed in high-power pulsed fiber lasers. The inset of the figure shows the laser spectrum that measured at the output power of 30 W. The emission wavelength was centered at 2017 nm with a FWHM (full width at half maximum) width of ~11 nm. This spectrum includes many peaks, showing that many longitudinal modes have oscillated in the cavity.

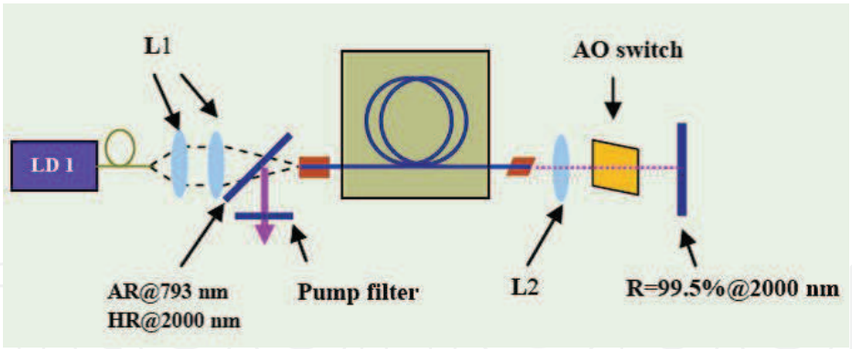

Fig. 4. Experimental setup for the AO Q-switched TDFL.

As shown in Fig. 5, the output power shows a linear dependence on the pump power at the high RR (50 kHz). However, at lower RRs, such as 10 kHz, the output power curve shows a severe deviation from linearity (not shown here), *i.e.*, there is a rollover of the output power curve. This rollover indicates that strong ASE was generated in the fiber and was emitted from both fiber ends. In order to achieve linear power dependence at lower RRs, such as 10 kHz, high diffraction-efficiency AO modulators are required. The appearance of ASE also put a limit on the maximum pulse energy that can be obtained in Q-switched fiber lasers. Further increasing the pump power just improves the ASE, and the Q-switched operation will become less effective.

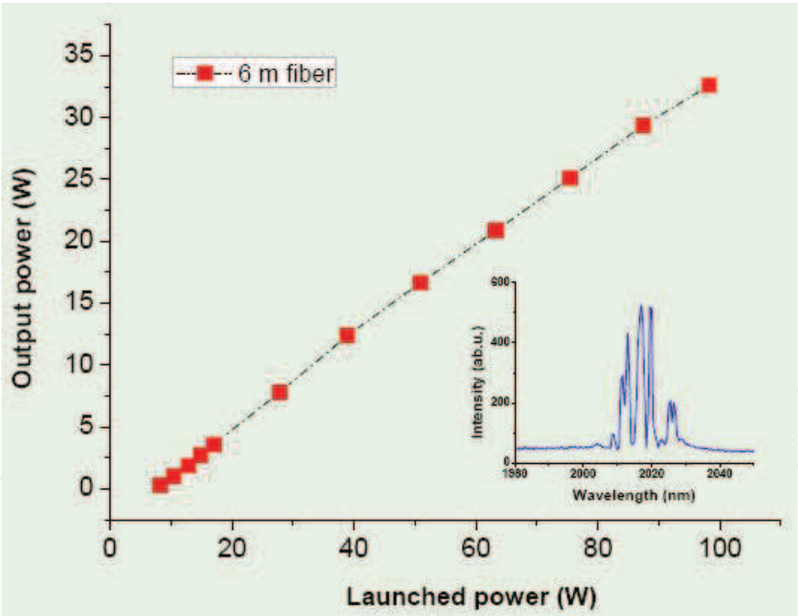

Fig. 5. Average output of the 6-m AO Q-switched TDFL.

Inset is the laser spectrum measured at the 30-W output level.

In pulsed fiber lasers, the RR usually has influence on the average output power when pump power is fixed. We measured the average power of the 6-m TDFL at a constant pump lever (50 W pump power) under different modulation frequencies, and the results are

shown in Fig. 6. The maximum output power only shows little decrease when the RR decreases from 50 kHz to 20 kHz. However, when the RR further decreases to less than 20 kHz, the average power indicates a significant drop (over 20%). Therefore, the AO modulation frequency only has significant impact on the Q-switched TDFL when it is operated at low RRs. The pulse train recorded under the RR of 10 kHz is shown in Fig. 7, indicating somewhat low inter-pulse instability.

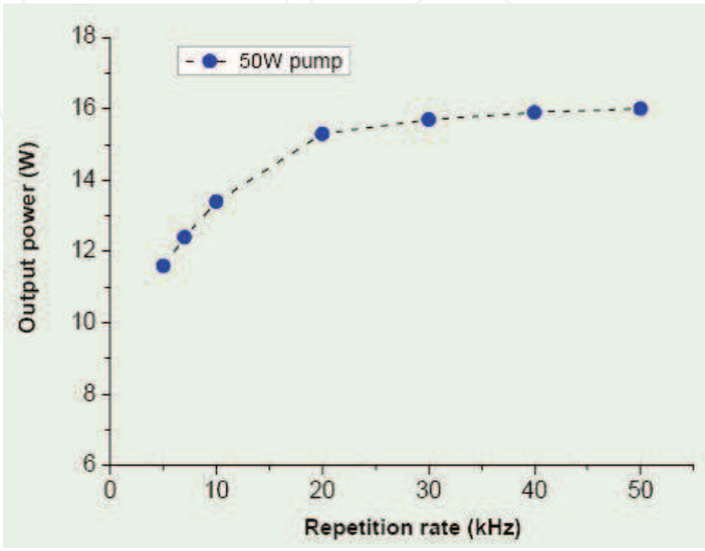

Fig. 6. Average output of the 6-m AO Q-switched TDFL under constant pump power but different RRs.

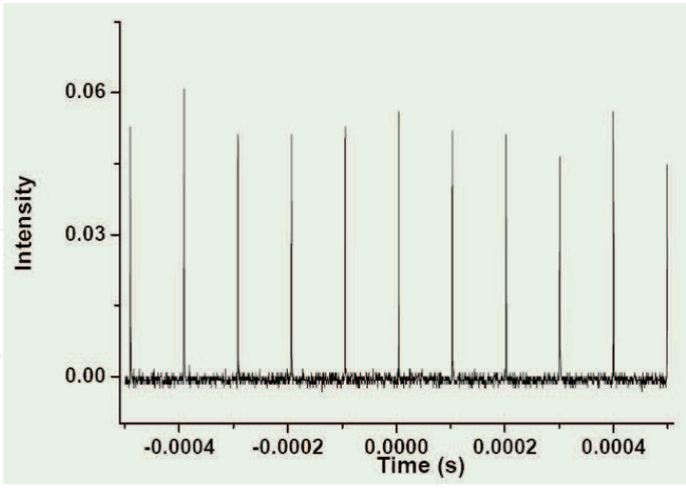

Fig. 7. Pulse train of the 6-m AO Q-switched TDFL at the RR of 10 kHz.

Operated under the RR of 10 kHz, the recorded pulse shape under different pump levels are shown in Fig. 8, where Pt denotes the threshold pump power. Just at the threshold, the laser pulse has a smooth shape with a pulse FWHM width of 240 ns. With increasing pump power, the pulse width narrows, and multiple peaks appears in the pulse. In a review description, Wang *et al*. proposed that the multi-peak pulse was initiated from the injection

of ASE by quick switching of the AO modulator and the subsequent evolution of the switching-induced perturbation [35].

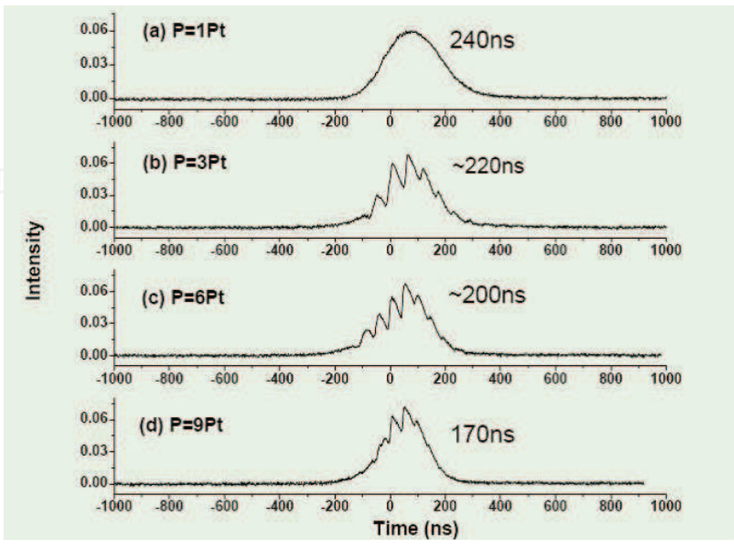

Fig. 8. Pulse evolution of the fiber laser at 10 kHz under different pump levels.

2.2 Pulse narrowing of Tm^{3+}-doped fiber lasers

For Q switched fiber lasers, the laser pulse width can be expressed as [36]

$$\tau_p = \frac{r\eta(r)}{r-1-\ln r} \times \frac{2L}{c\delta_0}, \tag{1}$$

where, δ_0 is the single-pass cavity loss, $\eta(r)$ is the energy extraction efficiency, r is the pump ratio (the ratio of the pump power to the threshold power), and L is the cavity optical length. Equation (1) implies that we can narrow the pulse duration through either increasing the pump strength r or shortening the fiber length. Simple calculations of the influence of the pump ratio on pulse narrowing are shown in Figs. 9 and 10, where $A = \frac{r}{r-1-\ln r}$ corresponding to the pulse width parameter. As shown in Fig. 9, the pulse width can be narrowed by a factor of ~6.3/1.5=4.2 when the pump ratio is increased from 2 to 10. When the pump ratio is over 10, further increasing the pump strength, such as from 10 to 100 (Fig. 10), can hardly shorten the pulse width to a appreciate level.

Based on the above analysis, we made an effort to obtain 2-μm laser pulse as narrow as possible from an AO Q-switched TDFL. For this aim, we shortened the fiber length to 0.4 m and increased the pump ratio as high as possible to carry out the Q-switching operation of the TDFL. With this fiber length, the maximum average output power was less than 2 W due to the fiber-length induced limited pump absorption. At a constant RR of 10 kHz, the pulse width narrowing characteristic with absorbed pump power is shown in Fig. 11. With increasing pump power, the pulse width reduces significantly. However, when the pump power was larger than 14 W, further increasing pump cannot lead to pulse narrowing. The shortest pulse width achieved with this 0.4-m TDFL was ~48 ns, as shown in the inset of Fig. 11.

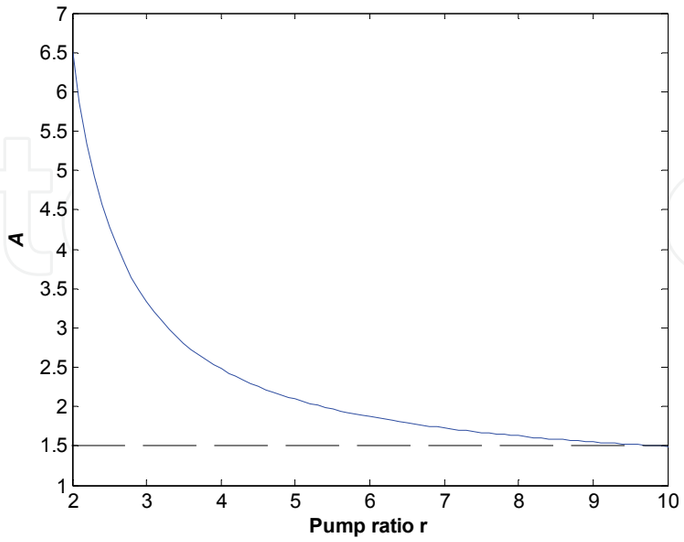

Fig. 9. Simulated evolution of the pulse width narrowing factor as a function of pump ratio from 2 to 10.

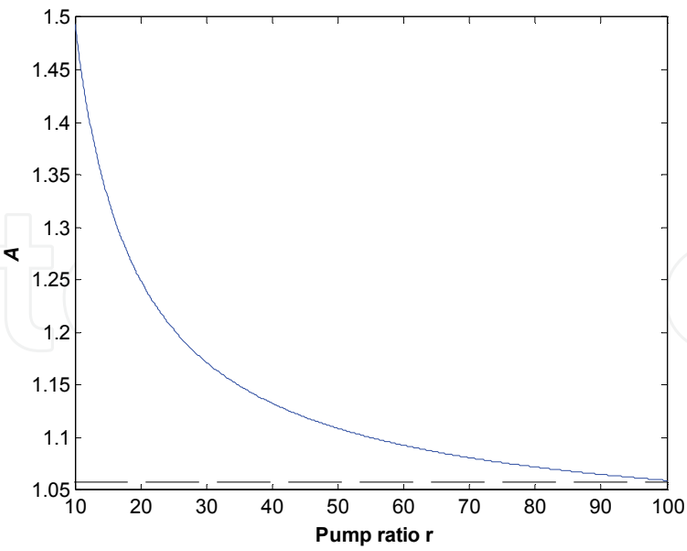

Fig. 10. Simulated evolution of the pulse width narrowing factor as a function of pump ratio from 10 to 100.

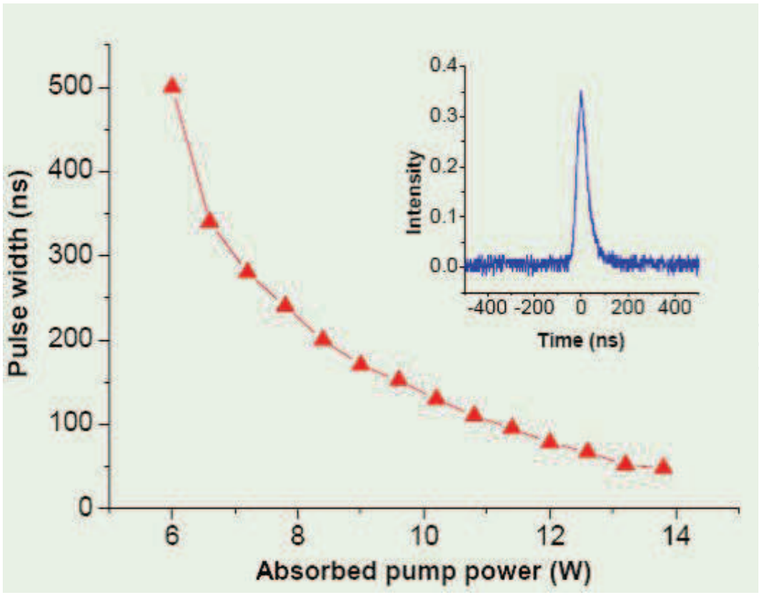

Fig. 11. Pulse width of the 0.4-m TDFL as a function of the absorbed pump.

Inset is the pulse shape with a width of ~48 ns.

Compared with bulk pulsed lasers, pulsed fiber lasers can provide higher average power due to their intrinsic high gain. However, it is still difficult to construct high-power 2-μm pulsed TDFLs at present. The difficulties mainly lie in the low damage threshold of the facets of fiber ends or other optical elements, and the onset of ASE. Therefore, how to improve the damage threshold of related optical components and efficiently suppress ASE will be the key problems for achieving high-power pulsed 2-μm TDFLs.

3. Gain-switching operation of Tm^{3+}-doped fiber laser

3.1 High-power gain-switching 2-μm fiber laser

With active Q-switching crystal lasers, stably controlled pulsed laser output can be achieved. With fiber amplifying systems, high gain can be easily obtained. Therefore, combining these two techniques is a potential way to scale 2-μm pulsed laser power to a new level. Besides, the advantages of high-doping concentration, efficient pump absorption, and long exited-state lifetime of Tm^{3+} fibers provide excellent prerequisites to achieve high-power pulsed 2-μm laser output.

In conventional fiber amplifiers, the seed source power is usually low. With such kind of seed source, a multi-stage fiber amplifier system must be constructed to achieve high average output power. The whole system is thus complicated and expensive. When the seed source has a narrow linewidth, the amplified output power of the fiber amplifier will be limited by the onset of stimulated Brillouin scattering (SBS). Ch. Ye *et al*. proposed using self-phase modulation (SPM) induced linewidth broadening to suppress SBS, and have obtained 50-W average power from a fiber amplifier [37]. For amplification of broad band ~2-μm laser pulses in Tm^{3+} fibers (~20 nm), SBS suppression is not a serious issue.

For obtaining 2-μm laser pulse, gain-switched fiber lasers can be excellent candidates owing to the well controlled pump pulse width and various available pump wavelengths. Gain-switched operation of TDFLs has achieved pulse energy of more than 10 mJ [38-40] and pulse width as narrow as 10 ns [41]. Compared with fiber amplifier systems, gain-switched devices can provide a more compact system configuration.

At present, actively Q-switched crystal lasers can provide moderate-power (several watts) 2-μm laser pulse with stably controlled characteristics. At the same time, TDFLs can provide high operation efficiency by taking advantage of the CR process [42-44]. Here, we will investigate how to improve the output from the pulsed TDFL through combining a high-power seed source with large-mode-area Tm^{3+} fiber amplification.

In experiment, we used a high-power Tm:YLF laser to gain switch the TDFL, which in turn was pumped by 793-nm LDs. This gain-switched system is different from conventional fiber amplifiers in that the high-power 'seed' laser acts just as a pulse switch, while the spectral characteristics are decided by the gain fiber. It is also different from conventional gain-switched lasers in that the gain and the switch are separated. We defined this laser system a combined gain-switched fiber laser (CGSFL) system. With this system, we will show how to achieve high-power 2-μm pulsed laser output through the combination of high-power switch laser, damage-threshold improvement of the fiber-end facts, and appropriate system configurations.

The experiment setup for the CGSFL system is shown in Fig. 12 [32]. The switch laser was an AO Q-switched Tm:YLF slab laser (pumped by a 793-nm LD) with the laser wavelength at 1914 nm. The Tm:YLF laser can provide a maximum average output power of ~4.4 W and RR from 500 Hz to 50 kHz. The pulse width can be varied between ~80 ns and ~1.2 μs by tuning the RR together with pump power. The 1914-nm laser pulse from the Tm:YLF laser was launched into the Tm fiber to switch the TDFL. The Tm^{3+}-doped silica fibers (both in the first-stage and the second-stage) had a ~25-μm diameter, 0.1-NA core doped with ~2wt.% Tm^{3+}. The octagonal pure-silica inner cladding had a 400-μm diameter and a NA of 0.46.

In the first-stage CGSFL, the pump source was a 120-W LD module at 793 nm. Two aspheric lenses (L1) were used to couple the 793-nm pump light into the gain fiber, with a coupling efficiency of ~80%. In this stage, a 6-m Tm^{3+} fiber was adopted with total pump absorption of ~18 dB. The amplified laser beam from the first stage was then launched into the second-stage Tm^{3+} gain fiber for further power scaling. In the second stage, the pump source was a ~230-W 793-nm LD module. The Tm^{3+} fibers were wrapped on 10-cm-diameter copper drums, which in turn were cooled by 18-°C circulating water.

In the first-stage CGSFL system, we launched ~1-W switch laser beam (with a pulse width of ~400 ns) into the fiber and kept the RR at 10 kHz. Under maximum pump power, this amplification stage can provide a maximum 2-μm pulsed laser of ~40 W with a slope efficiency of 50%. The maximum pulse energy was about 4 mJ, corresponding to a peak power of ~10 kW. At this level, no fiber facet damage was observed.

For amplification in the second stage (4-m Tm^{3+} fiber), the output of the first stage was kept at 15 W and the pulse RR was kept at 50 kHz. The laser output characteristics from the

second stage Tm^{3+} fiber are shown in Fig. 13 [32]. The maximum output is ~105 W (pulse energy of 2.1 mJ) with a slope efficiency of 52.8%. When we decreased the RR to 40 kHz, the output power dropped down to ~100 W (corresponding to pulse energy of 2.5 mJ), and the fiber end facet was damaged. At this time, the pulse width was measured to be ~600 ns, leading to pulse peak power of ~4.2 kW.

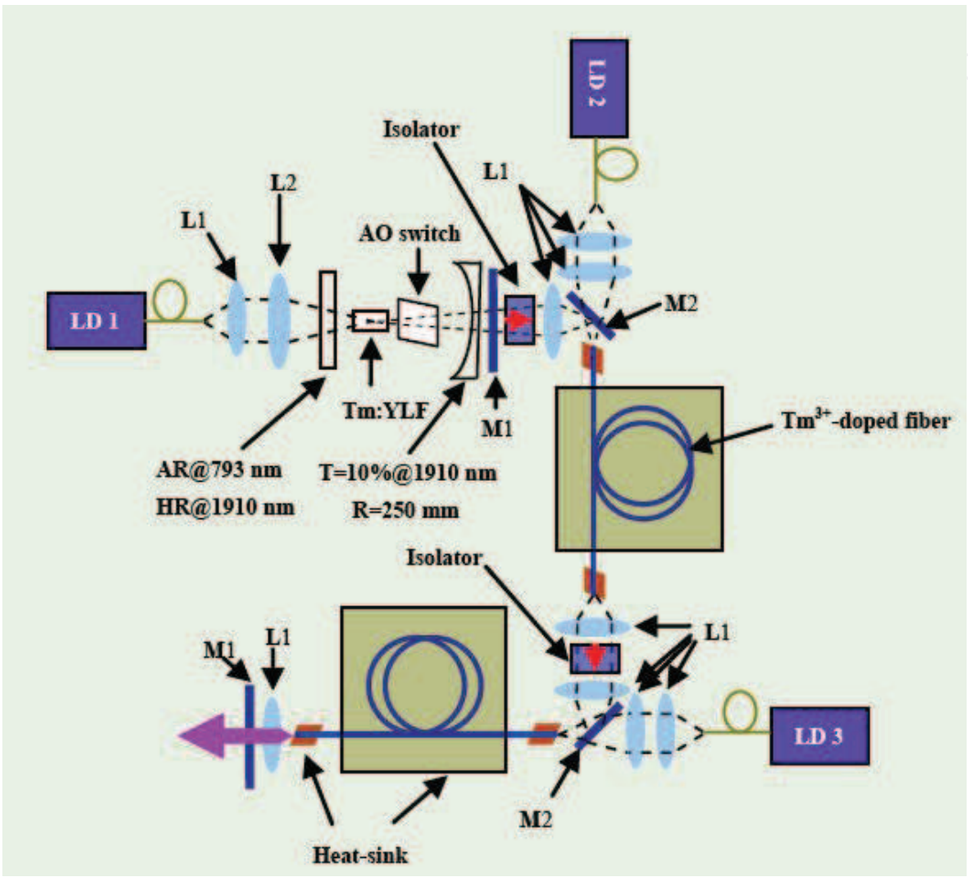

Fig. 12. Experimental setup of the combined gain-switched Tm^{3+}-fiber laser.
LD: laser diode; AR: anti-reflection; HR: high reflection; AO: acousto-optic;
L1: aspheric lens with f=11 mm; L2: convex lens with f=40 mm; M1& M2: dichroic mirrors.

In order to obtain higher output laser pulse energy, we fusion spliced a short piece (~2 mm) of passive silica fiber (1-mm diameter) to both ends of the active Tm fiber. At this time, only the first-stage CGSFL system (6-m fiber) was employed. We decreased the pulse RR to 500 Hz and kept the seed power at 200 mW. The maximum amplified ~2-μm output power was ~5.2 W, corresponding to a pulse energy of 10.4 mJ. The 1-mm-diameter endcaps greatly decreased the optical fluence at the output facet (<5 J/cm^2), which is less than the measured surface-damage fluence for nanosecond pulses in silica [45]. According to the empirical damage threshold for fused silica [46] of >22$t_P^{0.4}$ J/cm^2 (t_P is the pulse width in ns), the damage threshold of the 1-mm endcap facet would be hundreds of mJ. Therefore, this CGSFL system has the potential to scale the ~2-μm pulse energy even higher.

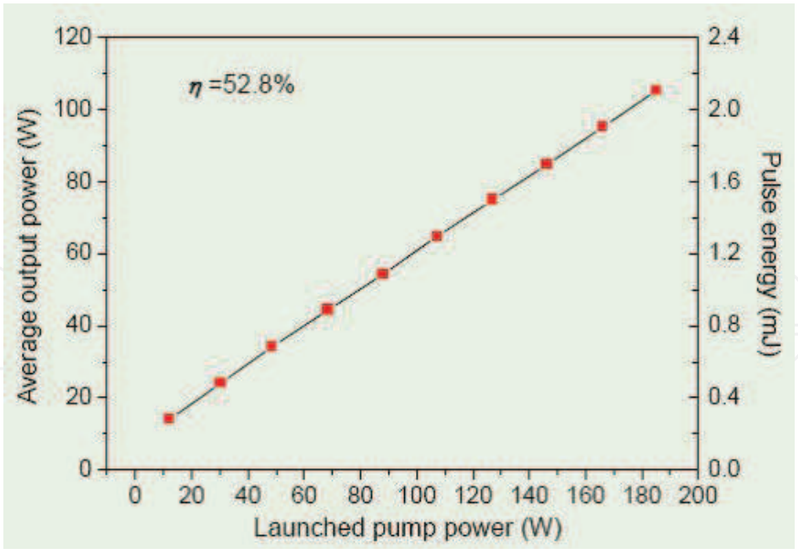

Fig. 13. Amplified output power from the two-stage CGSFL system at 50 kHz.

Under different RRs, the maximum average power and pulse energy achieved with this CGSFL system are shown in Fig. 14 [32]. The maximum output power increases near linearly with RR. Over 40 kHz, the roll-over of the average output was owing to the limited pump. On the other hand, the maximum pulse energy first decreases sharply with RR and then almost saturates due to limited stored energy. The inset is the pulse shape measured at the pulse energy of ~10 mJ with a FWHM width of 75 ns, corresponding to a peak power of ~138 kW.

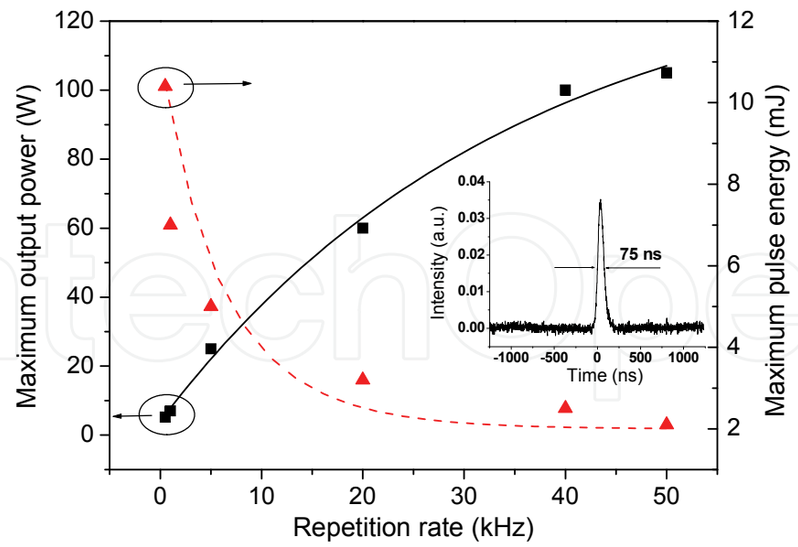

Fig. 14. Maximum average output power and pulse energy of the CGSFL system as a function of RR.

With the two-stage CGSFL system, the evolution of the 2-μm pulse shape (50 kHz) is shown in Fig. 15 [32]. The switch laser was kept at 1 W and had a pulse width of 900 ns. With

increase of output power, the pulse width increased first and then narrowed, accompanied by steepening of the pulse leading edge. At 100-W power level, the pulse width was reduced to 750 ns, corresponding to pulse narrowing of ~17%. The pulse broadening at low power levels was probably originated from coexistence of the switch pulse and the ~2020-nm laser pulse (see Fig. 16). The pulse width narrowing and pulse steepening at high power levels was attributed to gain saturation and self-phase modulation [47-49].

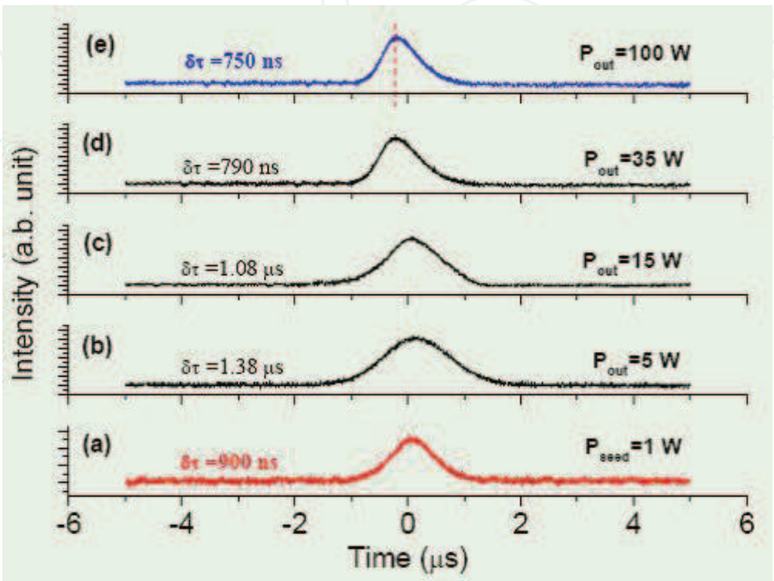

Fig. 15. Characteristics of the switch pulse and the fiber laser pulse at different power levels. (a)-(d) were measured after the first-stage CGSFL and (e) was measured after the second-stage CGSFL.

Under the same operating conditions (50-kHz RR and 1-W seed power), the spectrum of the seed and the output pulse at various power levels are indicated in Fig. 16 [32]. The fluorescence spectrum of the Tm^{3+}-doped fiber is also shown in Fig. 16(a). It is clear that the 1914-nm seed laser was amplified at comparatively low power levels. When the 1914-nm laser was near 5 W, the ~2-μm laser pulse was stimulated, and thereafter more and more stored energy was extracted by the 2020-nm laser pulse. Finally, all energy was included in the 2020-nm laser beam. This is a unique characteristic of the CGSFL system, significantly different from fiber amplifiers and singly gain-switched devices. The detailed process can be described as follows. Owing to the broad fluorescence spectrum of our Tm fiber (1920-2040 nm), the switch pulse (1914 nm) lies in the wing of the gain spectrum. When the switch laser was launched into the fiber core, more than 90% of the laser was absorbed. At the same time, the Tm fiber accumulated population inversion through 793-nm pumping. The unabsorbed 1914-nm laser pulse will be amplified, while the absorbed 1914-nm laser pulse will modulate the gain of the system and act as a switch for the ~2-μm laser. Gain competition between the 1914-nm amplification and the stimulation of the ~2-μm laser emission leads to the evolution of the spectrum. Eventually, the 1914-nm laser was consumed completely and all stored energy was extracted by the ~2-μm laser emission. At 100-W level, the spectral width of the ~2-μm laser pulse was ~25 nm. We also observed the spectral evolution of a 2-m Tm^{3+} fiber laser with one-stage CGSFL configuration, and found that shorter fibers need stronger pump to switch on the CGSFL system.

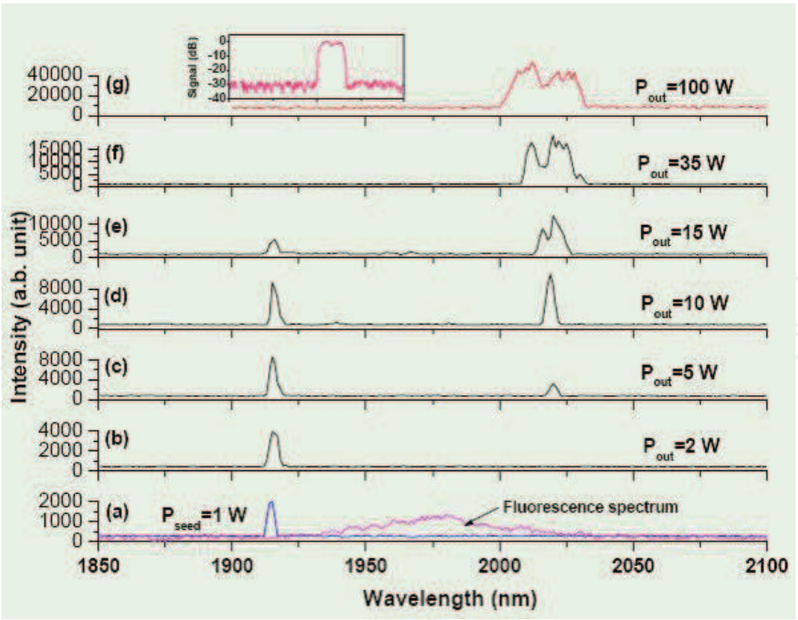

Fig. 16. Laser spectra (blue line) of the switch pulse (a), and that of the fiber laser pulse (b-f) at different power levels of the CGSFL system. (a) also shows the fluorescence spectrum of the Tm fiber.

3.2 Resonant-pumping 2-μm fiber laser

In high-power ~2-μm fiber lasers, the pump source is usually 790-nm LDs. Great difference between the pump wavelength and the laser wavelength causes a high quantum defect. This makes the optical-optical transfer efficiency of TDFLs be generally lower than that of high-power Yb fiber lasers. In order to improve the quantum efficiency thus the slope efficiency of high-power TDFLs, the pump wavelength must be elongated toward the laser wavelength. Such a pumping scheme with the pump wavelength approaching the laser wavelength is defined as resonant pumping. Resonant pumping TDFLs with ~1.6-μm wavelength has achieved slope efficiencies of ~80% with tens of miliwatts output [50].

In the pulsed 2-μm TDFLs achieved either by Q-switching [24] or by mode-locking [51], the laser power and pulse energy were usually limited. We have shown in the previous section that gain-switched TDFLs can produce high pulse energies, but their slope efficiencies were still low. Besides, the output pulses of these gain-switched TDFLs consist of a series of relaxation spikes, showing great chaotic temporal characteristics. In order to eliminate the chaotic spiking in gain-switched fiber laser, we must adopt highly-resonant pulsed pumping scheme, which is named as fast gain switching [52].

The experimental setup for the fast gain-switched TDFL is shown in Fig. 17 [53]. The pump source was an AO Q-switched Tm:YLF laser with 8.5-W maximum output at 1.914 μm. The M^2 beam quality of the pump beam was ~2. The double-clad Tm^{3+}-doped silica fiber had a ~30-μm diameter, 0.09 NA (numerical aperture) core doped with Tm^{3+} of ~2wt.% concentration. The pure-silica D-shape inner cladding had an average diameter of 400 μm

and a NA of 0.46. One aspheric lens (f = 11 mm) was used to couple the pump light into the fiber core, with a coupling efficiency of ~90%. The absorption coefficient of the Tm^{3+} fiber at the pump wavelength (1914 nm) was measured with the cut-back method to be ~3 dB/m. At the output fiber end, a dichroic mirror (R=90%@1914nm & T=75%@1940nm, 45° coated) was used to filter the un-absorbed 1914-nm pump light. The 1940-nm laser output was calibrated by subtracting the un-filtered pump light and incorporating the filter-mirror-rejected laser light.

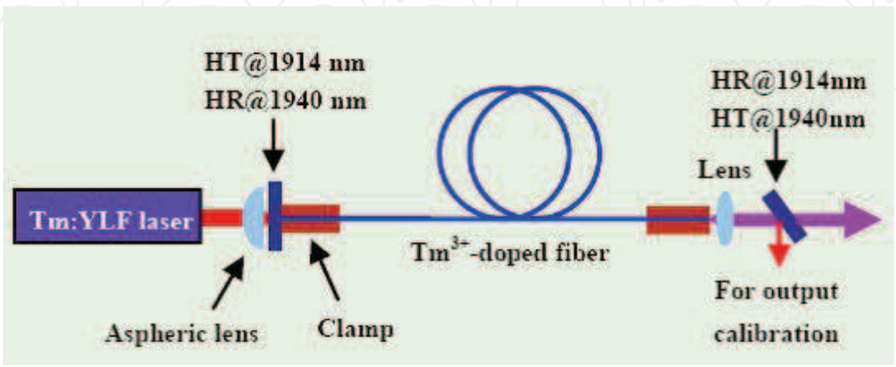

Fig. 17. Experimental setup of the resonantly gain-switched TDFL. HT: high transmission; HR: high reflection.

In experiment, three fiber lengths of 2, 4, and 6 m were used. Pumping at 1914 nm directly excites the Tm^{3+} ions from the ground state $^3H_6$ to the upper laser level $^3F_4$, which has a lifetime of ~340 μs [10]. The comparatively long lifetime of the upper laser level and the quasi-three-level nature of the laser transition guarantee efficient operation of the system through resonant pumping.

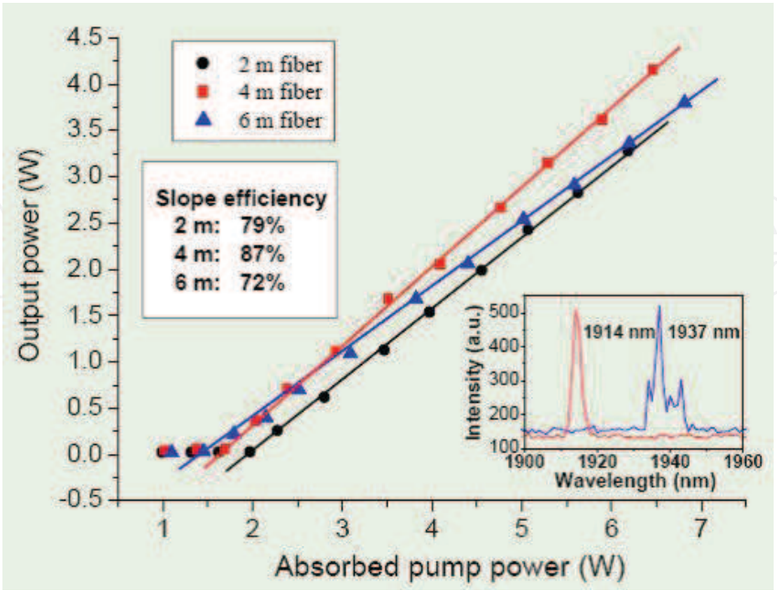

Fig. 18. CW Output performance of the resonantly-pumped TDFL.
Inset shows the laser spectra of the output laser beam and the pump light.

CW operation characteristics of the TDFLs (with the Q switch turned off) are shown in Fig. 18 [53]. The 4-m fiber provided a maximum output of 4.14 W and a slope efficiency of 87% with respect to absorbed pump power. Slope-efficiency dropping of the 6-m fiber can be attributed to laser re-absorption, while slope-efficiency reduction of the 2-m fiber mainly originated from the comparatively lower laser reflection coefficient of the pump-end dichroic mirror for the 2-m TDFL (1933 nm) than the 4-m TDFL (1937 nm). The figure inset shows the laser spectrum of the 4-m TDFL at 4-W output level, together with that of the 1914-nm pump source. The laser wavelength was center at 1937 nm, with a total FWHM width of ~7 nm and a main-transition-peak FWHM width of ~2.5 nm. Simple calculation shows that such a laser system only has a quantum defect of 1.4%.

When the Tm:YLF laser was Q-switched, the TDFL would be operated in the gain-switched mode. In order to achieve stable gain-switched 2-μm TDFLs, fast gain switching is required, i.e., the pump source must be able to realize a fast buildup of population inversion, which is depleted by only one signal pulse. Pumping the Tm^{3+} fiber with 790 nm, fast gain switching cannot be realized owing to the long relaxation time (>10 μs) from the pump level $^3H_4$ to the laser emission level $^3F_4$ [54], which will leads to relaxation spiking. On the other hand, if the TDFL is directly pumped to the laser emission band, population inversion can be built up instantaneously with the pump pulse, leading to the cavity gain being switched on and off in the same time scale as the pump pulse. Therefore, an AO Q-switched Tm:YLF laser at ~1.9 μm was chosen to pump the TDFL, and the pump pulse width was kept at ~120 ns. Output laser pulses of the 4-m gain-switched TDFL at RR of 10 and 20 kHz are shown in Fig. 19 [53]. It can be seen that single laser pulse is clean with no relaxation spiking present.

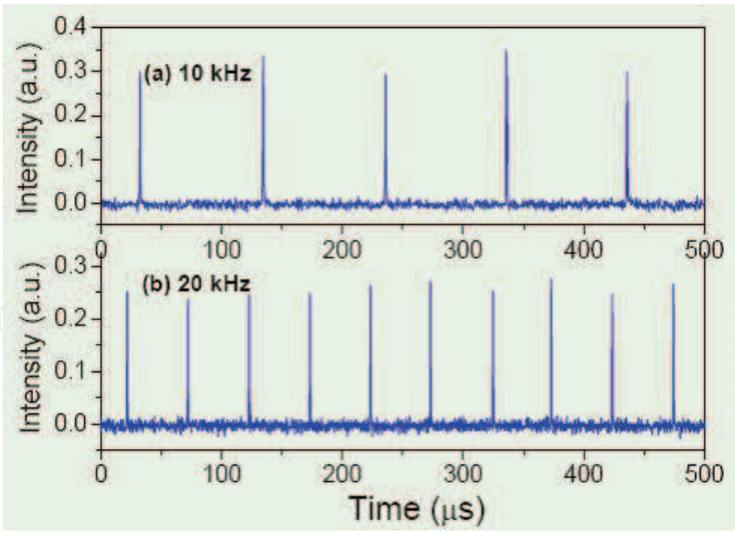

Fig. 19. Pulse trains of the 4-m gain-switched TDFL at the RR of (a) 10 kHz and (b) 20 kHz.

Laser output characteristics of the gain-switched TDFL under the RR of 20 kHz are shown in Fig. 20 [53]. The average output power was measured by adding up the output from both fiber ends, but the pulse energy was calculated only by dividing the far-fiber-end output by the RR. The optimum fiber length is also 4 m. The 4-m TDFL produced a maximum average power of 4 W and pulse energy of 0.155 mJ.

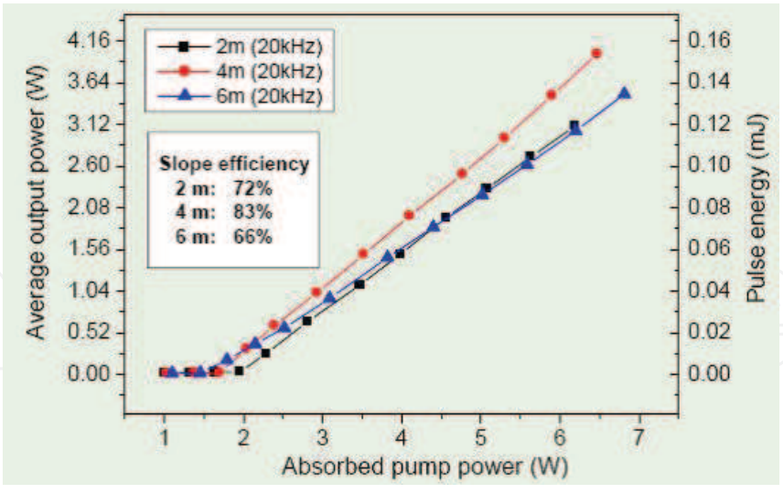

Fig. 20. Pulsed operation performance of the gain-switched TDFLs with different fiber lengths at the RR of 20 kHz.

In order to further scale pulse energy of the gain-switched TDFL, we kept the 4-m fiber laser near the maximum pump level and decreased the RR. Both average output power and pulse energy were measured only at the far fiber end, and the results are shown in Fig. 21 [53]. The average power tended to saturates at high RR. The maximum pulse energy reached 1.3 mJ at 2 kHz, and the pulse FWHM width was 61 ns, corresponding to peak power of ~21.3 kW.

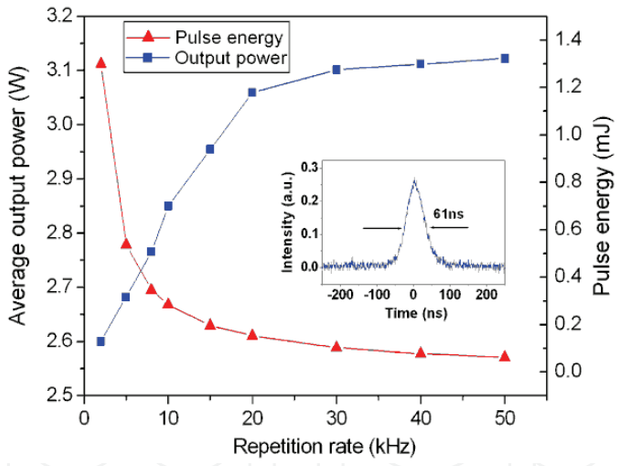

Fig. 21. Average power and pulse energy of the 4-m TDFL as a function of RR. Inset is the pulse shape measured near the maximum output power.

Due to high light density in fiber core, the peak power and pulse energy of TDFLs are still limited by optical damage and occurrence of nonlinear optical effects. Therefore, how to improve the pulse energy of 2-μm TDFLs is still a very important issue in the near future.

4. Self-pulsing operation of Tm^{3+}-doped fiber laser

When Tm^{3+} ions are doped into the medium such as glass, every energy manifold will be further split to many sub energy levels (Stark splitting). Therefore, TDFLs can produce

fluent dynamical behaviors, including relaxation oscillation, self-pulsing, and self-mode-locking [55, 56]. Some of the dynamical behaviors can be advantages, but some others may be disadvantages. Among all kinds of the dynamical behaviors happened in TDFLs, self-pulsing phenomenon may be the most interesting one.

4.1 Self pulsing in Tm^{3+}-doped fiber lasers

It's well known that self-pulsing can be achieved in any laser with an adequate saturable absorber [57]. Self pulsing in TDFLs has been extentively observed, and was thought to result from saturable absorption due to ion-pair clusters, up-conversion and excited-state absorption (ESA) processes, or strong interactions among longitudinal modes [55,56,58–60]. In free running operation, the TDFL will operate successively in CW mode, self-pulsing mode and again CW mode with continuous increase of the pump power [61].

First, we construct a free-running laser configuration with a piece of Tm^{3+}-doped fiber to observe the formation and evolution of self-pulsing in TDFLs with increasing pump power. The experimental arrangement is shown in Fig. 22. The Tm^{3+}-doped fiber laser is pumped by a 40-W pig-tailed LD centered at ~792 nm. The Tm fiber has a 30-μm diameter, 0.22 NA core doped with Tm^{3+} of ~2 wt.% concentration. The inner cladding had a 410 μm diameter and a NA of 0.46. The fiber length used is 6 m. The dichroic mirror at the pump end and the far-end perpendicularly cleaved fiber facet (~3.55% Fresnel reflection) formed a Fabry-Perot cavity.

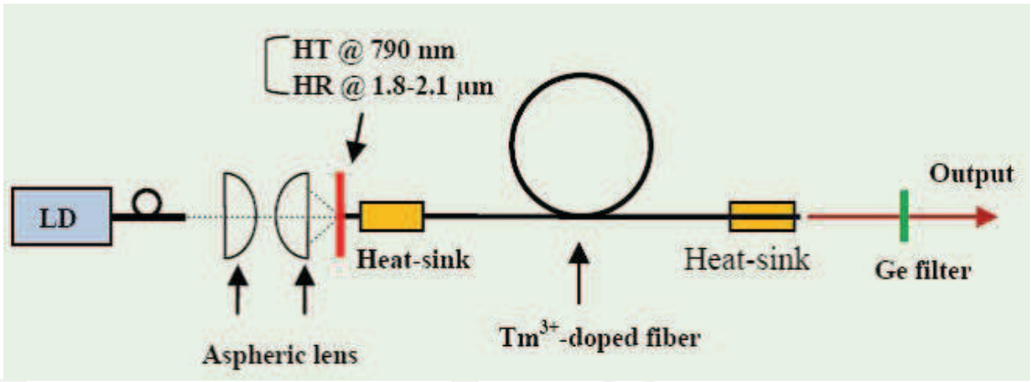

Fig. 22. Experimental arrangement of LD-pumped Tm^{3+}-doped fiber laser

The threshold pump power of the fiber laser is slightly less than 10 W. Increasing the pump power continuously, the fiber laser can operate at several stages. The evolution of the self-pulsing characteristics of the fiber laser is shown in Fig. 23. When the pump power is near the threshold (P=10 W), the laser delivers a regular train of pulses. When the pump power is increased to 12 W, the self-pulsing train is still high regular, and the pulse width narrows and the pulse frequency increases. Increasing the pump power over 15 W, the pulsing operation is randomized, and more like mode locking. When the pumping level is even higher (25 W), the laser output becomes quasi-CW.

The pulse width and frequency of the 6-m self-pulsing TDFL as a function of pump power are indicated in Fig. 24. At slightly over the pump threshold, the pulse width and pulse frequency, decreases and increases sharply with pump power respectively. When the pump power is over 14 W, the pulse width and pulse frequency show a near linear change with

increasing pump power. At high pump levels, e.g. over 25 W, the pulse width begins saturating. Therefore, it is hard to further narrowing the pulse duration of self-pulsing TDFLs just through increasing pump power.

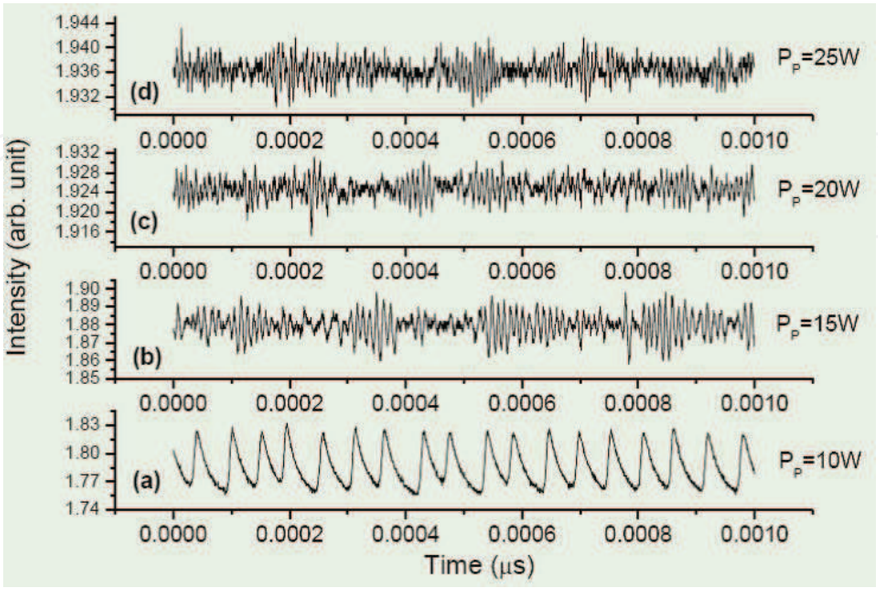

Fig. 23. Output intensity time trace of 6 m fiber laser with the end-facet output coupler for various pump powers.

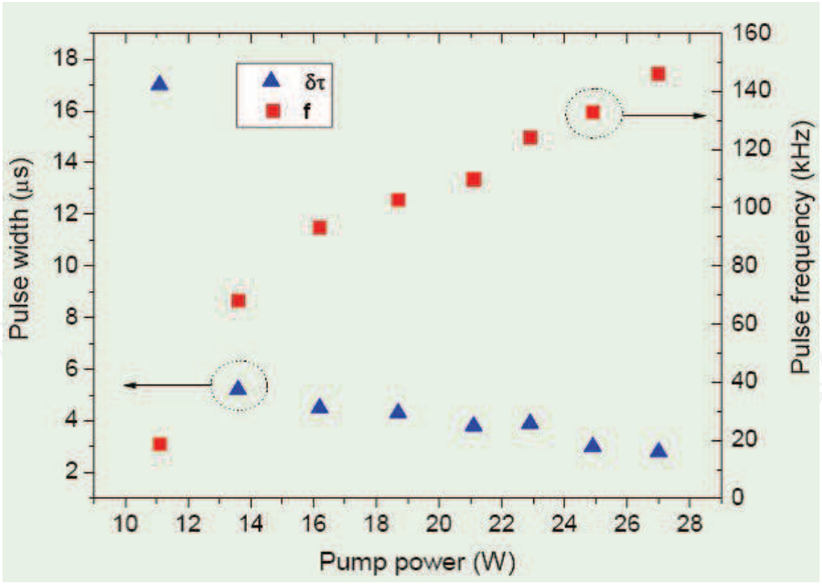

Fig. 24. Pulse width and pulse frequency versus pump power.

When the transmission of the output coupler is changed, the self-pulsing characteristics will be somewhat different. In order to make a efficient comparison of pulse width and frequency with different couplers, we define a intracavity laser power (equals to the output power divided by the coupling value). Three kinds of output couplers are used in the experiment:

T=5%, *T*=20%, and *T*=96% (the fiber facet). The dependence of the pulse width and frequency on the output coupler transmission (*T*) under different pump power is shown in Fig. 25.

It is clear that the pulse width decreases first sharply and then slowly with the intra-cavity power, which is in agreement with the description in the literature [62]. With increasing intra-cavity power level, the T=20% coupler shows much less change compared with the other two couplers, implying that self-pulsing operation can be sustained in a wider pump range. We suppose there is a optimum output coupling value that can support large-range self-pulsing operation.

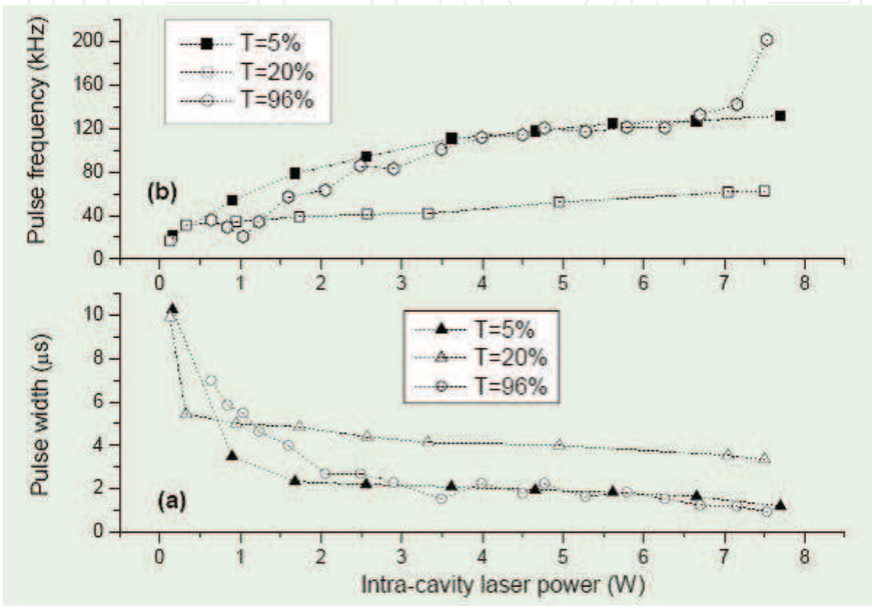

Fig. 25. Output coupling dependence of (a) pulse width and (b) pulse frequency under different intra-cavity power levels.

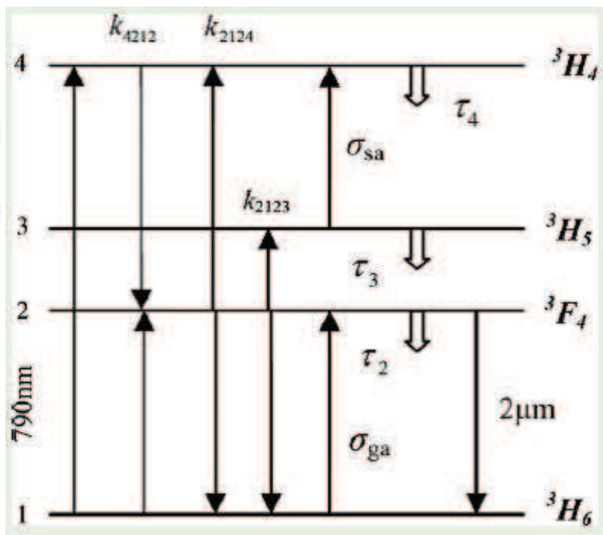

Fig. 26. Schematic of the four lowest energy manifolds in Tm^{3+} ions.

For Tm^{3+}-doped fiber lasers, as shown in Fig. 26 [63], the pump light at 790 nm excites the ions from $^3H_6$ state to $^3H_4$ state, which quickly relaxes to the upper laser level $^3F_4$. In heavily Tm^{3+}-doped fibers, the distance between Tm^{3+} ions decreases, strengthening the interaction between ions. This strong inter-ion interaction provides a loss mechanism, depopulating the 2-μm transition level $^3F_4$. This kind of loss mechanism acts as a saturable absorber, leading to the formation of self-pulsing. However, what is the real loss mechanism responsible for self-pulsing in the TDFL?

4.2 Origin of self-pulsing in Tm^{3+}-doped fiber lasers

Many mechanisms have been proposed to explain the origin of self-pulsing in TDFLs, but consistent agreement has not been reached yet. In this section, we will try to find out the real reason accounting for the self-pulsing formation in TDFLs through theoretical analysis and numerical simulation.

For Tm^{3+} ions, the energy-level structure diagram is sketched in Fig. 26, including several important transition and energy-transfer processes. The rate equations for the local population densities of these levels are as follows [64-66]

$$\begin{aligned}\frac{dN_4}{dt} &= R(z,t)(N_1 - N_4) - k_{4212}N_1N_4 \\ &\quad + k_{2124}N_2^2 - \frac{N_4}{\tau_4} + \sigma_{sa}c\phi(z,t)(N_3 - N_4)\end{aligned}, \tag{2}$$

$$\begin{aligned}\frac{dN_3}{dt} &= k_{2123}N_2^2 + \beta_{43}\frac{N_4}{\tau_4} - \frac{N_3}{\tau_3} \\ &\quad - \sigma_{sa}c\phi(z,t)(N_3 - N_4)\end{aligned}, \tag{3}$$

$$\begin{aligned}\frac{dN_2}{dt} &= 2k_{4212}N_1N_4 - 2(k_{2124} + k_{2123})N_2^2 + \beta_{42}\frac{N_4}{\tau_4} \\ &\quad + \beta_{32}\frac{N_3}{\tau_3} - \frac{N_2}{\tau_2} - c\phi(z,t)\sigma_e(N_2 - \frac{g_2}{g_1}N_1) \\ &\quad + c\phi(z,t)\sigma_{ga}(N_1 - N_2)\end{aligned}, \tag{4}$$

$$\begin{aligned}\frac{d\phi}{dt} &= c\phi(z,t)\sigma_e(N_2 - \frac{g_2}{g_1}N_1) + m\frac{N_2}{\tau_2} \\ &\quad - \sigma_{ga}c\phi(z,t)(N_1 - N_2) - r_c\phi(z,t)\end{aligned}, \tag{5}$$

$$N_1 = N_{tot} - N_2 - N_3 - N_4\,, \tag{6}$$

$$R(z,t) = R(0,t)\cdot e^{-\alpha_p \cdot z}\,, \tag{7}$$

where N_i are the populations of four energy manifolds $^3H_6$, $^3F_4$, $^3F_5$, $^3H_4$, and N_{tot} is the total density of Tm^{3+} ions. R is the pump rate, and ϕ is the average photon density of the laser field. σ_e is the stimulated emission cross section of signal light, σ_{ga} and σ_{sa} are the absorption cross sections of ground state and excited state, respectively. Where g_1 and g_2 are the

degeneracies of the upper and lower laser levels, τ_i is the level lifetimes of four manifolds, and r_c is the signal photon decay rate. β_{ij} are branch ratios from the i to j level, m is the ratio of laser modes to total spontaneous emission modes. The coefficients k_{ijkl} describe the energy transfer processes: k_{4212} and k_{3212} are the cross relaxation constants, and k_{2124} and k_{2123} are the up-conversion constants. The coefficient a_p is the pump absorption of the fiber, which is calculated by $\alpha_p = \sigma_{ap} \cdot N_{tot}$, where σ_{ap} is the pump absorption cross section. In the analysis and simulation, the phonon-assisted ESA process of $^3F_4$, $^3H_5 \rightarrow {}^3H_6$, $^3H_4$ and ground-state absorption (GSA) through the $^3F_4$, $^3H_5 \rightarrow {}^3H_6$, $^3F_3$ energy transfer process are considered. The corresponding parameters are listed in Table 1 [66-68].

Parameter	numerical value
k_{4212}	1.8×10^{-16} cm^{3}s^{-1}
k_{2123}	1.5×10^{-18} cm^{3}s^{-1}
k_{2124}	1.5×10^{-17} cm^{3}s^{-1}
τ_i	$\tau_4 = 14.2\mu s$ $\tau_3 = 0.007\mu s$ $\tau_2 = 340\mu s$
β_{ij}	$\beta_{43} = 0.57$ $\beta_{42} = 0.051$ $\beta_{32} \approx 1$
σ_e	2.5×10^{-21} cm^2
σ_{sa}	Variable (4×10^{-21} cm^2)
σ_{ga}	variable
m	8×10^{-7}
r_c	9.7×10^6 s^{-1}
σ_{ap}	1×10^{-20} cm^2
N_{tot}	1.37×10^{20}cm^{-3}

Table 1. The parameters in the rate equations

Theoretical calculation

Provided the lifetime of level N_3 (0.007 μs) is much shorter than that of level N_2 (340 μs), we simplify the energy manifolds to three levels, i.e. we assume N_3~0 and let $N_{23} = N_2+N_3$. By adding Eq. (3) and (4), we get

$$\begin{aligned}\frac{dN_{23}}{dt} &= 2k_{4212}N_1N_4 - (2k_{2124}+k_{2123})N_{23}^2 + (\beta_{43}+\beta_{42})\frac{N_4}{\tau_4} - \frac{N_{23}}{\tau_2} \\ &\quad -c\phi[\sigma_e(N_{23} - \frac{g_2}{g_1}N_1) + \sigma_{sa}(N_{23}-N_4) - \sigma_{ga}(N_1 - N_{23})]\end{aligned} \quad (8)$$

Then, the rate equations are simplified to a three-level system. Suppose the laser operating in the steady-state (or CW) regime, i.e. $\frac{d\phi}{dt}=0$ and $\frac{dN_i}{dt}=0$, we can solve ϕ, N_1 and N_{23} from the Eqs. (2), (5) and (8). Through solving the equations, we found that there was a certain pump range (defined as ΔR), where the steady-state solution for the rate equations could not be found. In this range, the laser would not be operated in the CW state. With increase or decrease of pump power out of the range ΔR, the operation of Tm^{3+}-doped fiber lasers would undergo phase transition (changed to CW operation). Such a case is in good agreement with the experimental observation in the self-pulsing TDFLs.

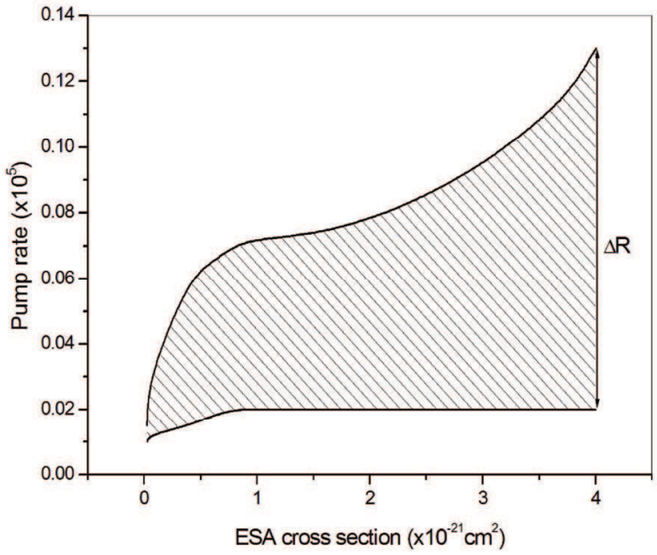

Fig. 27. The non-CW pump range ΔR as a function of the ESA cross section.

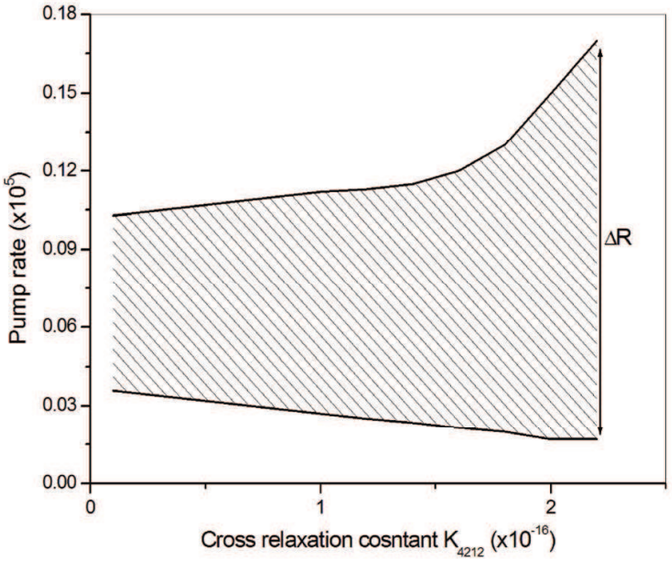

Fig. 28. The non-CW pump range ΔR as a function of the cross relaxation strength.

Then the non-CW range ΔR was calculated as varying the ESA cross section and the cross relaxation parameter k_{4212}. The variation of ΔR as a function of the ESA cross section is shown in Fig. 27 [63]. The non-CW range ΔR increases with the ESA cross section, especially increases exponentially when the ESA cross section is larger than 3×10^{-21} cm^2. When the ESA cross section is less than 1×10^{-21} cm^2, the range ΔR shrinks sharply, and goes to zero with a small value of ESA cross section. The CW operation of TDFLs can sustain for any pump rate when the ESA cross section is sufficiently small. On the other hand, with a larger ESA cross section, the CW operation will always be broken.

The non-CW range ΔR calculated as a function of the cross relaxation strength k_{4212} is shown in Fig. 28 [63]. Large values of k_{4212} will obviously enlarge the range ΔR. However, even when the cross relaxation k_{4212} is decreased to zero, the breaking of CW operation still preserves, implying that the cross relaxation process is not the key factor in the formation of self-pulsing in TDFLs.

Simulation results

The revolution of the photon density in TDFLs is investigated through numerical simulation based on the complete rate equations (2-7). In the simulation, four energy-transfer processes (cross relaxation, energy transfer up-conversion, GSA and ESA) are calculated separately to analyze their influence on the formation of self-pulsing.

The impact of the cross relaxation is evaluated by varying the value of the parameter k_{4212}. The simulation results are shown in Fig. 29 [63]. Stable CW laser operation preserves whatever value of k_{4212} is adopted. With the increase of k_{4212}, the laser intensity will be increased. Therefore, strong cross relaxation process may be helpful for improving the slope efficiency of TDFLs, but cannot account for the formation of self-pulsing.

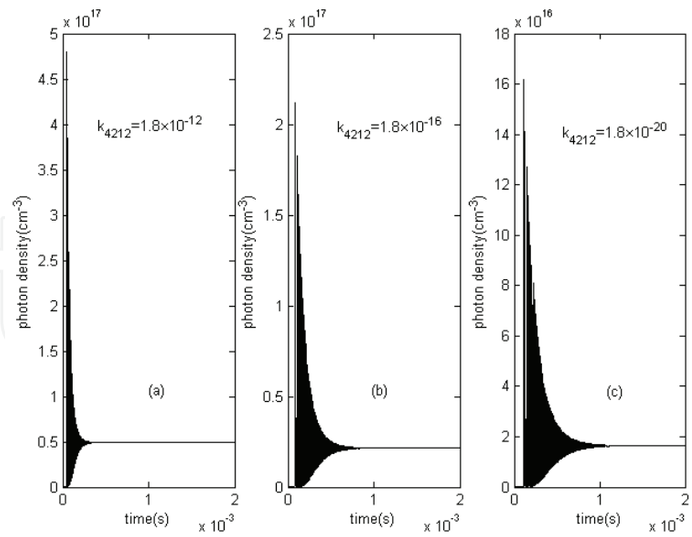

Fig. 29. Laser photon density dynamics characteristics with different cross-relaxation strength k_{4212}.

Then, we numerically observed the influence of the energy-transfer up-conversion process $^3F_4$, $^3F_4 \rightarrow {}^3H_6$, $^3H_5$ (k_{2123}) and $^3F_4$, $^3F_4 \rightarrow {}^3H_6$, $^3H_4$ (k_{2124}). The simulation results for k_{2124} are shown in Fig.

30 [63]. When the up-conversion is too strong, *i.e.*, k_{2124}>1.5×10^{-16} cm^{3}s^{-1}, the laser relaxation oscillation is suppressed, as shown in Fig. 30(a-c). The photon density is clamped in a very low level. When the parameter k_{2124}<1.5×10^{-17} cm^{3}s^{-1}, the laser relaxation oscillation occurs again. No matter which values of the parameters (from 1.5×10^{-6} cm^{3}s^{-1} to zero) are chosen, no self-pulsing phenomenon is observed. The behaviors of the parameters k_{2123} are very similar to that of k_{2124}. The up-conversion process does not directly connect to the self-pulsing operation in TDFLs. In the practical Tm^{3+}-doped system, the values of k_{2123} and k_{2124} are around 10^{-17} - 10^{-18} cm^{3}s^{-1}. The main influence of up-conversion is increasing the laser threshold.

The GSA is also called as the re-absorption in the Tm^{3+}-doped fiber lasers, which had been thought as a possible mechanism for the self-pulsing formation. The GSA process $^3H_6 \rightarrow {}^3F_4$ can be thought as a reverse process of the laser transition $^3H_6 \rightarrow {}^3F_4$. We kept the emission cross section σ_e constant and changed the value of g_2/g_1. The GSA strength increases with a larger value of g_2/g_1. When g_2/g_1=0, the fiber laser is a complete four-level system; when g_2/g_1=1, the fiber laser corresponds to a complete three-level system. In simulation, we changed the g_2/g_1 value from 0 to 1 to study the evolution of photon density, and found that stable CW operation always occurs. Therefore, the GSA process is definitely not the cause of the self-pulsing in TDFLs.

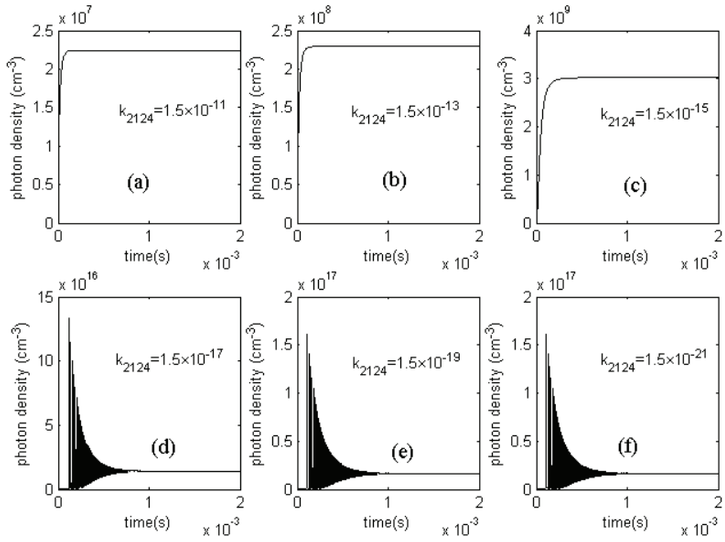

Fig. 30. Laser photon density dynamics characteristics with different energy-transfer up-conversion strength k_{2124}.

When only the ESA process $^3H_5 \rightarrow {}^3H_4$ is taken into account, the revolution of photon densities for various ESA cross sections σ_{sa} are shown in Fig. 31 [63]. When the ESA cross section σ_{sa} is chosen in the range from 4×10^{-21} to 4×10^{-19} cm^2, it is clear to observe stable, regular self-pulsed trains. This verifies the theoretical predication that the ESA process is the key reason leading to the self-pulsing dynamics in TDFLs. When the ESA cross section σ_{sa} is much small, the ESA is too weak to hinder accumulation of the population in the level $^3H_5$ (N_3), and CW operation occurs after relaxation oscillation. With the increase of the ESA cross section σ_{sa}, the decay time of the relaxation oscillation becomes longer and longer, and finally, the relaxation oscillation evolves to a stable self-pulsed train.

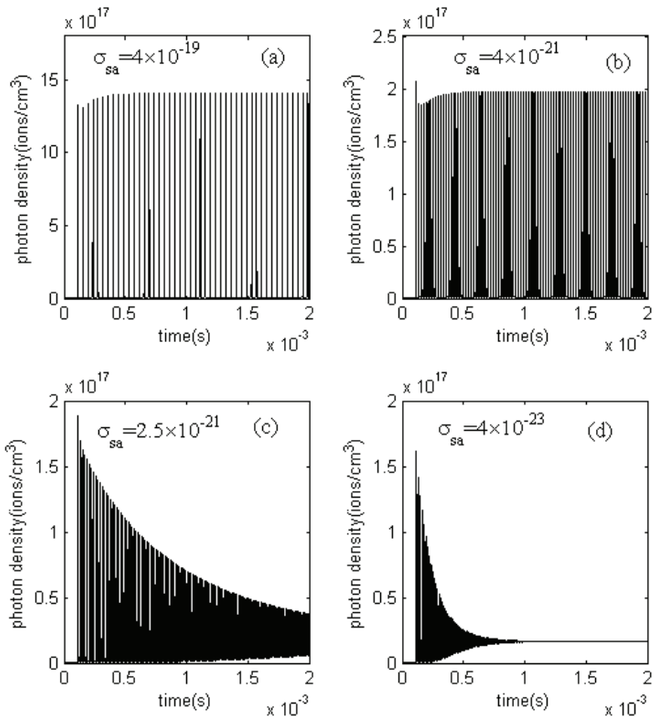

Fig. 31. Laser photon density dynamics characteristics with different ESA strength σ_{sa} (cm²).

4.3 Theoretical model and self-pulsing behaviors in Tm^{3+}-doped fiber lasers

Theoretical model

The schematic of our theoretical model to simulate the beam propagation in the Tm^{3+}-doped fiber is depicted in Fig. 32 [69]. The theoretical model is constructed based on the above mentioned rate equations (2) to (7), and the value of ESA cross section σ_{sa} is fitted from our experimental observations.

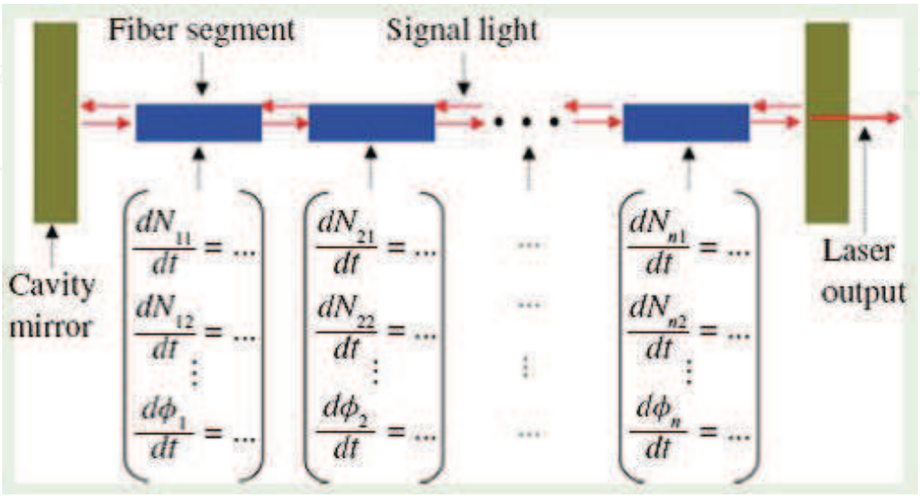

Fig. 32. Schematic of the simulation model.

The laser field S(z) propagating along the fiber can be expressed as follows:

$$\frac{dS_{f,b}(z)}{dz} = \pm S_{f,b}(z)[\sigma_e \Delta N(z) - \sigma_{sa} N_3(z) - \delta_s], \tag{9}$$

where the subscripts f and b denoting the forward and backward directions, respectively; δ_s is the intrinsic absorption of the host glass at the laser wavelength (set at 2.3×10^{-3} m^{-1}), and $\Delta N = N_2 - \frac{g_2}{g_1} N_1$.

The boundary conditions for the laser field are given by

$$S_b(L) = R_{S2} S_f(L), \; S_f(0) = R_{S1} S_b(0), \tag{10}$$

where R_{S1} and R_{S2} are reflectivities of the front and rear mirrors at the pump and laser wavelength, respectively; L is the length of the fiber.

We divide the fiber into many segments and construct separate rate equations for every segment. The absorption of pump power along the fiber is calculated, and the pump power is converted to the pump rate in the rate equations. We digitize the rate equations in every segment with the Runge–Kutta method. Based on the propagation equation (9), the laser field at segment (t, z) propagates to segment ($t + \Delta t$, $z + \Delta z$). The whole set of digitalized equations are solved through the iterative approach.

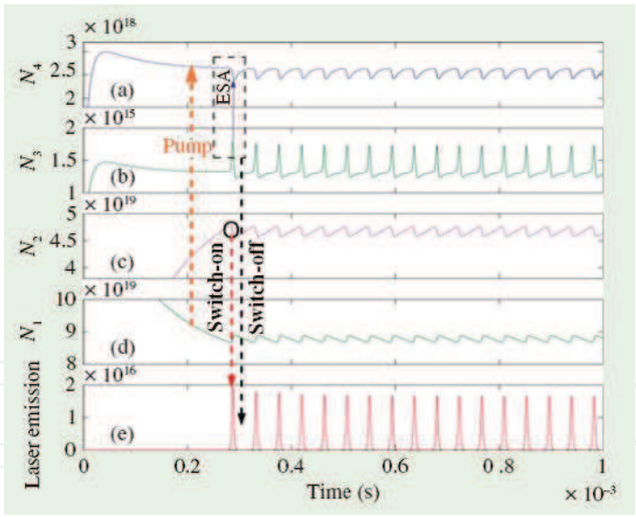

Fig. 33. Evolution of the populations of the four lowest energy manifolds of the Tm^{3+}-doped fiber laser and that of the corresponding laser emission.

Based on the theoretical model, the evolution of the populations of the four lowest energy manifolds of Tm^{3+} ions and the 2-μm signal photon density were simulated, and the results are shown in Fig. 33 [69]. The formation of self-pulsing can be explained as follows. When the fiber is pumped, the population N_1 of the ground-state level ($^3H_6$) is excited to the $^3H_4$ level (N_4). Through nonradiative transition and cross relaxation, the population jumps to the $^3H_5$ level (N_3) and $^3F_4$ level (N_2). After a time delay of ~0.28 ms, the photon density increases

sharply, leading to the occurrence of laser emission, as shown by the first pulse in Fig. 33(e). At the same time, the population of N_3 increases and N_4 decreases simultaneously, leading to drop in the population difference N_4-N_3. This aggravates the ESA process [$^3H_5$ (N_3)$\rightarrow$$^3H_4$ (N_4)], hindering the accumulation of the population inversion ΔN ($N_2-N_1 g_2/g_1$). Consequently, the laser emission is switched off by the ESA process ($^3H_5\rightarrow{}^3H_4$). After the laser emission is switched off, the population N_4 and the population inversion ΔN will be pumped up once more. The laser occurs again when the cavity loss is overcome by the gain for another time. This switching on and off process will operate repeatedly, accounting for the formation of self-pulsing.

Figure 34 shows the numerically calculated self-pulsing train of the TDFL near the threshold pump rate. This regular self-pulsing train has a pulse width and RR of 7.68 μs and 16.89 kHz, respectively, being in good agreement with experimental results.

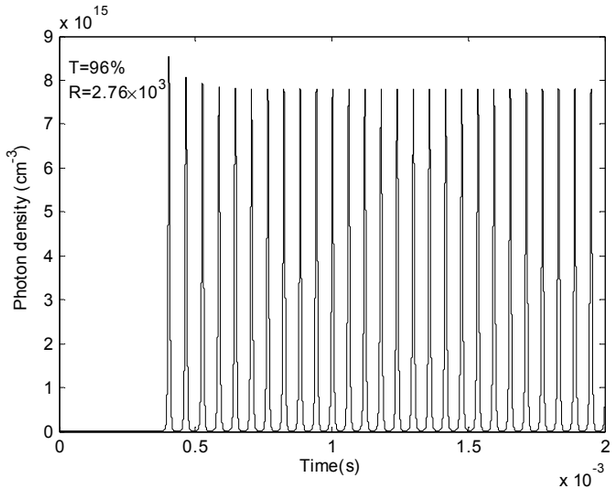

Fig. 34. Self-pulsing train at corresponding threshold pump rate with output coupling T=96%.

Influence of several parameters on the self-pulsing characteristics

With self-pulsing threshold pump strength, the laser pulse width and pulse frequency as a function of output coupling are shown in Fig. 35 [69]. The pulse frequency increases and the pulse width decreases nearly exponentially with the output coupling. Compared with the simulation results, the experimental observation shows slightly higher pulsing frequencies and narrower pulse widths. By using higher output coupling, higher pump level is needed to sustain self-pulsing. In such a case, accumulation of population inversion and switching of N_3 and N_4 populations by the ESA process are faster than that achieved by using lower output coupling, leading to higher pulse frequency and narrower pulse width.

To compare the simulation with the experimental results, we normalized the pump rate (power) to their corresponding threshold values, which is defined as the pump ratio $r=R/R_P$ (in simulation) or $r=P/P_{th}$ (in experiment). In the self-pulsing regime, the pulse width and pulse frequency as a function of r are depicted in Fig. 36 [69]. The pulse frequency and the pulse width display reverse tendencies with the increase of pump ratio. At high pump

ratios, both pulsing frequency and pulse width tend to saturate. With r=3 in the experiment, the pulse width decreases to 0.8 μs, and the pulse frequency increases to 110 kHz, respectively. In the simulation, the maximum pulse frequency can be as high as 900 kHz with the minimum pulse width of about 200 ns (not shown here).

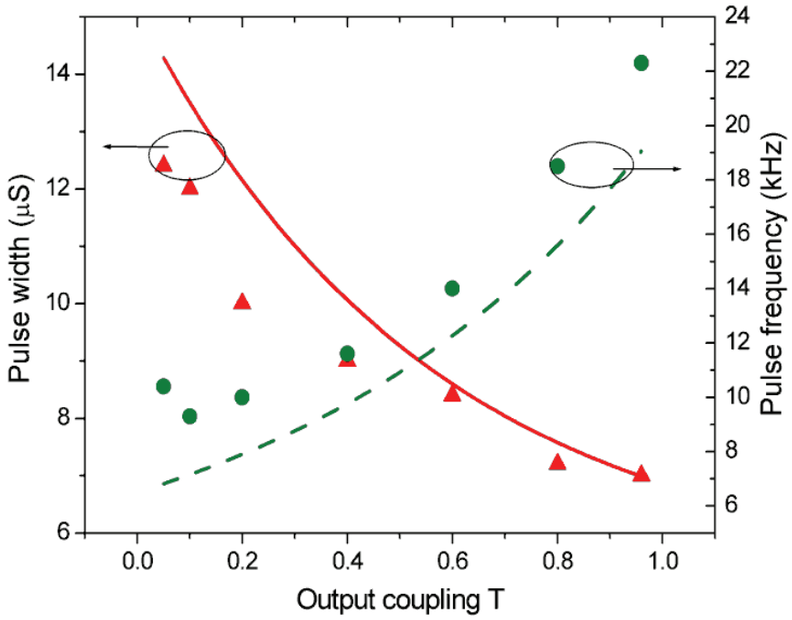

Fig. 35. Pulse width and frequency of the SP Tm^{3+}-doped fiber laser with various output couplings at the respective threshold pump levels. The solid and dotted lines show the simulation results, and the triangle and diamond dots indicate the experimental results.

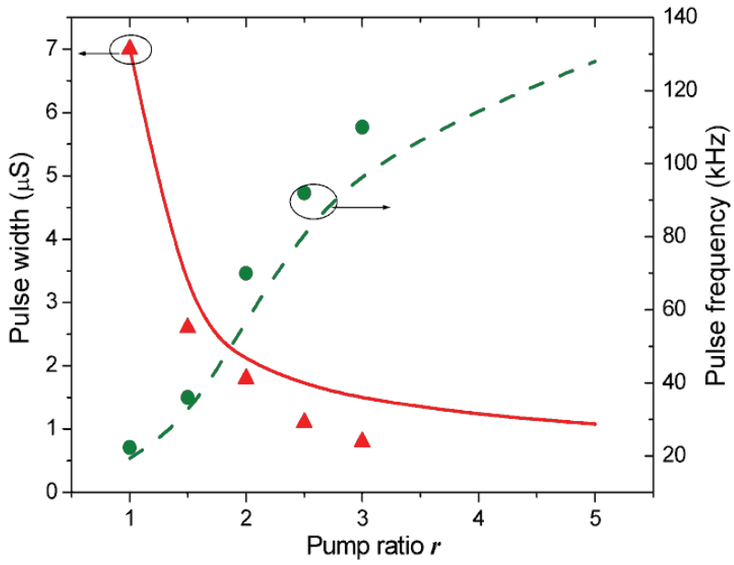

Fig. 36. Pulse width and pulse frequency of the Tm^{3+}-doped fiber laser with T~96% output coupler at various pump levels. The solid and dotted lines show the simulation results, and the triangle and circle dots indicate the experimental results.

In TDFLs, appropriately high Tm^{3+} doping concentration can strengthen the cross relaxation process, which significantly enhances the quantum efficiency of the laser.

Here, the SP operation is examined by changing the Tm^{3+} doping concentration in unit ppm (part per million). In experiment, Tm^{3+} doping concentration of ~1150 ppm [55] and ~2100 ppm were adopted. The pulse frequency and width as a function of Tm^{3+} doping concentration are shown in Fig. 37 [69]. As the Tm^{3+} concentration increases from ~1000 ppm to ~15000 ppm, the pulse frequency grows from 15 to ~110 kHz, and the pulse width narrows exponentially to ~350 ns and saturates. Higher doping concentration strengthens the CR, EUC, and re-absorption processes. The combination of these processes can speed up the recovery of population inversion after the pulse is switched off, thus improving the pulse frequency and narrowing the pulse width. Higher doping concentration is preferred to simultaneously achieve high pulse frequency and narrow pulse. However, very high doping concentration may form Tm^{3+}-ion clusters in the silica fibers and cause serious concentration quenching. Consequently, a tradeoff exists between obtaining a narrow pulse width and high laser efficiency.

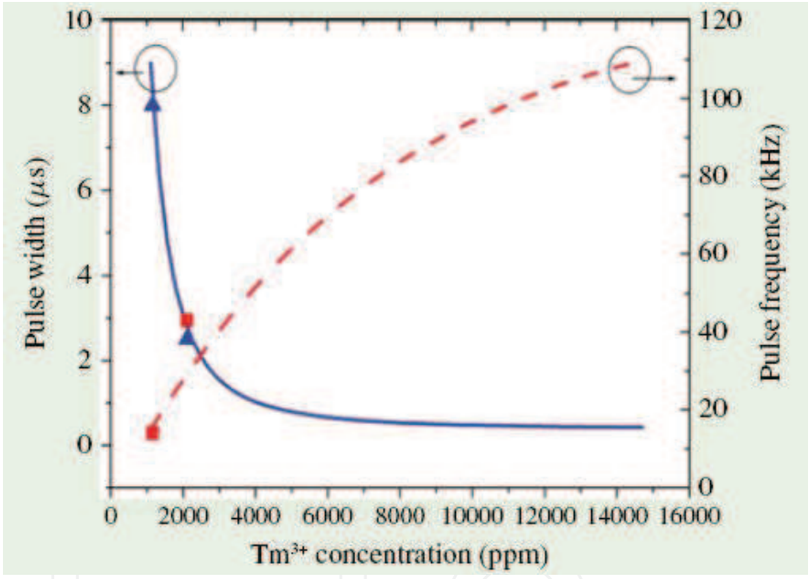

Fig. 37. Pulse width and frequency as a function of doping concentration at pump rate R=3.2×10^3 s^{-1}. The solid and dotted lines show the simulation results, and the triangle and rectangular dots indicate the experimental results.

Understanding the self-pulsing characteristics and methods as how to make use of it will help improving the performance and utility of 2-μm Tm^{3+}-doped fiber lasers.

5. Prospects of 2-μm Tm^{3+}-doped fiber lasers

Based on fast development of high-brightness laser diodes and optimizing of Tm^{3+} fiber fabrication technique, and further understanding about the spectral properties of Tm^{3+} ions, performance of TDFLs can be improved to a new stage. Due to its so many specific advantages, the Tm^{3+}-doped fiber laser has great potential in development toward high-power output, wide wavelength tunability, narrow pulse duration, and high peak power.

6. References

[1] P. Myslinski, X. Pan, C. Barnard, J. chrostowski, B. T. Sullivan, and J. F. Bayon, "Q-switched thulium-doped fiber laser," Opt. Eng. 32 (9), 2025-2030 (1993).

[2] L. Esterowitz, "Diode-pumped holmium, thulium, and erbium lasers between 2 and 3 μm operating CW at room-temperature," Opt. Eng., 29 (6): 676-680 (1990).

[3] R. C. Stoneman and L. Esterowitz, "Efficient, broadly tunable, laser-pumped Tm-YAG and Tm-YSGG CW lasers," Opt. Lett., 15 (9): 486-488 (1990).

[4] S. W. Henderson, P. J. M. Suni, C. P. Hale, S. M. Hannon, J. R. Magee, D. L. Bruns, and E. H. Yuen, "Coherent laser-radar at 2 μm using solid-state lasers," IEEE Trans. Geosci. Remote Sens., 31 (1): 4-15 (1993).

[5] I.T. Sorokina, K.L. Vodopyanov (Eds.): Solid-State Mid-Infrared Laser Sources, Topics Appl. Phys. 89, 219–255 (2003).

[6] H.W. Gandy, R.J. Ginther and J.F. weller, Stimulated emission of Tm3+ radiation in silicate glass, J. Appl. Phys. 38: 3030-3031 (1967).]

[7] R.G. Smart, J.N. Carter, A.C. Tropper and D.C. Hanna, "continuous-wave oscillation of Tm-doped fluorozirconate fibre laser at around 1.47m, 1.9 and 2.3 when pumped at 790nm", Opt. Commun. 82: 563-570 (1991).

[8] Jihong Geng, Jianfeng Wu, and Shibin Jiang, "Efficient operation of diode-pumped single-frequency thulium-doped fiber lasers near 2 μm," Opt. Lett., 32 (4): 355-357 (2007).

[9] N. Y. Voo, J. K. Sahu, and M. Ibsen, "345-mW 1836-nm Single-Frequency DFB Fiber Laser MOPA," IEEE Photon. Technol. Lett. 17, 2550 (2005).

[10] Jianqiu Xu, Mahendra Prabhu, Jianren Lu, Ken-ichi Ueda, and Da Xing, "Efficient double-clad thulium-doped fiber laser with a ring cavity," Applied Optics, 2001, 40(12): 1983-1988.

[11] D.C. Hanna, I.M. Jauncey, R.M. Percival, I. R. Perry, R.G. Smart, P. J. Suni, J. E. Townsend, A. C. Tropper: Continuous-wave oscillation of a monomode thulium-doped fibre laser, Electron. Lett. 24, 1222 (1988).

[12] W. L. Barnes, J.E. Townsend: Highly tunable and efficient diode pumped operation of Tm3+ doped fibre lasers, Electron. Lett. 26, 746 (1990).

[13] J. N. Carter, R.G. Smart, D.C. Hanna, A.C. Tropper: CW diode-pumped operation of 1.97 μm thulium-doped fluorozirconate fibre laser, Electron. Lett. 26, 599 (1990).

[14] Jackson, S.D., and King, T.A.: 'High-power diode-cladding-pumped Tm-doped silica fiber laser', Opt. Lett., 1998, 23, pp. 1462–1464.

[15] R.A. Hayward, W.A. Clarkson, P.W. Turner, J. Nilsson, A.B. Grudinin and D.C. Hanna, Efficient cladding-pumped Tm-doped silica fibre laser with high power singlemode output at 2μm, Electron. Lett., 36 (8): 711-712 (2000).

[16] G. Frith, D.G. Lancaster and S.D. Jackson, "85W Tm3+-doped silica fibre laser," Electron. Lett., 41, 687-688 (2005).

[17] Y. Jeong, P. Dupriez, J. K. Sahu, J. Nilsson, D. Shen, and W. A. Clarkson, "Thulium-ytterbium co-doped fiber laser with 75 W of output power at 2 μm," SPIE, 5620: 28-35 (2004).

[18] Evgueni Slobodtchikov, Peter F. Moulton, Gavin Frith, "Efficient, High-Power, Tm-doped Silica Fiber Laser," 2007ASSP-MF2.

[19] P. F. Moulton, G. A. Rines, E. V. Slobodtchikov, K. F. Wall, G. Frith, B. Samson, and A. L. G. Carter, "Tm-Doped Fiber Lasers: Fundamentals and Power Scaling," IEEE J. Sel. Topics in Quantum Electronics, 15 (1): 85-92 (2009).
[20] T. Ehrenreich, R. Leveille, I. Majid, and K. Tankala, "1 kW, all-glass Tm:fiber laser," in Proc. SPIE Photonics West 2010: LASE Fiber Lasers VII: Technology, System and Applicatons, San Francisco, CA, Jan. 2010, Paper 7580.
[21] G. D. Goodno, L. D. Book, and J. E. Rothenberg, "low-phase-noise single-frequency single mode 608 W thulium fiber amplifier," Opt. Lett. 34 (8): 1204-1206 (2009).
[22] P. Myslinski, X. Pan, Ch. Barnard, et al., "Q-switched thulium-doped fiber laser," Opt. Eng. 32, 2025-2030 (1993).
[23] L.E. Nelson, E.P. Ippen, and H.A. Haus, "Broadly tunable sub-500 fs pulses from an additive-pulse mode-locked thulium-doped fiber ring laser," Appl. Phys. Lett. 67, 19-21 (1995).
[24] A.F. El-Sherif and T.A. King, "High-peak-power operation of a Q-switched Tm3+-doped silica fiber laser operating near 2μm," Opt. Lett. 28, 22-24 (2003).
[25] G. Imeshev and M. E. Fermann, "230-kW peak power femtosecond pulses from a high power tunable source based on amplification in Tm-doped fiber," Opt. Express 13(19), 7424–7431 (2005).
[26] B. C. Dickinson, S. D. Jackson, and T. A. King, "10 mJ total output from a gain-switched Tm-doped fibre laser," Opt. Commun. 182(1-3), 199–203 (2000).
[27] Y. J. Zhang, B. Q. Yao, Y. L. Ju, and Y. Zh. Wang, "Gain-switched Tm3+-doped double-clad silica fiber laser" Opt. Express 13 (2005) 1085-1089.
[28] M. Eichhorn and S. D. Jackson, "Actively Q-switched Tm3+-doped and Tm3+,Ho3+-codoped Silica Fiber Lasers," in Conference on Lasers and Electro-Optics and Quantum Electronics and Laser Science Conference 2008, (San Jose, CA, 2008).
[29] M. Eichhorn and S. D. Jackson, "High-pulse-energy actively Q-switched Tm3+-doped silica 2 μm fiber laser pumped at 792 nm," Opt. Lett. 32(19), 2780–2782 (2007).
[30] M. Eichhorn and S. D. Jackson, "High-pulse-energy, actively Q-switched Tm3+,Ho3+ -codoped silica 2 μm fiber laser," Opt. Lett. 33(10), 1044–1046 (2008).
[31] D. Creeden, P. Budni, and et al., "High Power Pulse Amplification in Tm-Doped Fiber," in Conference on Lasers and Electro-Optics, OSA Technical Digest (CD), paper CFD1 (Washington DC, 2008).
[32] Yulong Tang, Lin Xu, Yi Yang, and Jianqiu Xu, "High-power gain-switched Tm3+-doped fiber laser," Opt. Express 18, 22964 (2010).
[33] D. Creeden, P. A. Ketteridge, and et al., "Mid-infrared ZnGeP2 parametric oscillator directly pumped by a pulsed 2 microm Tm-doped fiber laser," Opt. Lett. 33(4), 315–317 (2008).
[34] R. J. De Young and N. P. Barnes, "Profiling atmospheric water vapor using a fiber laser lidar system," Appl. Opt. 49(4), 562–567 (2010).
[35] Y. Wang and Ch-Q. Xu, "Actively Q-switched fiber lasers: Switching dynamics and nonlinear processes" Progress in Quant. Electron. 31, 131-216 (2007).
[36] A. E. Siegman, LASERS, 1986, P492, P1017, Miller/Scheier Associates, Palo Alto, CA.
[37] Ch. Ye, M. Gong, P. Yan, Q. Liu, and G. Chen, "Linearly-polarized single-transverse-mode high-energy multi-ten nanosecond fiber amplifier with 50W average power," Opt. Express 14, 7604-7609 (2004).

[38] B. C. Dickinson, S. D. Jackson, and T. A. King, "10 mJ total output from a gain-switched Tm-doped fibre laser," Opt. Commun. 182(1-3), 199–203 (2000).
[39] Y. J. Zhang, B. Q. Yao, Y. L. Ju, and Y. Zh. Wang, "Gain-switched Tm3+-doped double-clad silica fiber laser," Opt. Express 13(4), 1085–1089 (2005).
[40] S. D. Jackson and T. A. King, "Efficient Gain-Switched Operation of a Tm-Doped Silica Fiber Laser," IEEE J. Quantum Electron. 34(5), 779–789 (1998).
[41] M. Jiang and P. Tayebati, "Stable 10 ns, kilowatt peak-power pulse generation from a gain-switched Tm-doped fiber laser," Opt. Lett. 32(13), 1797–1799 (2007).
[42] Y. L. Tang and J. Q. Xu, "Effects of excited-state absorption on self-pulsing in Tm3+-doped fiber lasers," J. Opt. Soc. Am. B 27(2), 179–186 (2010).
[43] G. Frith, D. G. Lancaster, and S. D. Jackson, "85 W Tm3+-doped silica fibre laser," Electron. Lett. 41(12), 687–688 (2005).
[44] S. D. Jackson, "Cross relaxation and energy transfer upconversion processes relevant to the functioning of 2 μm Tm3+-doped silica fibre lasers," Opt. Commun. 230(1-3), 197–203 (2004).
[45] B. C. Stuart, M. D. Feit, S. Herman, A. M. Rubenchik, B. W. Shore, and M. D. Perry, "Nanosecond-to-femtosecond laser-induced breakdown in dielectrics," Phys. Rev. B 53(4), 1749-1761 (1996).
[46] W. Koechner, "Solid-state laser engineering", 5th ed. P685. Springer-Verlag Berlin Heidelberg New York.
[47] E. C. Honea, R. J. Beach, S. B. Sutton, J. A. Speth, S. C. Mitchell, J. A. Skidmore, M. A. Emanuel, and S. A. Payne, "115-W Tm:YAG diode-pumped solid-state laser," IEEE J. Sel. Top. Quantum Electron. 33(9), 1592–1600 (1997).
[48] C. D. Brooks and F. D. Teodoro, "1-mJ energy, 1-MW peak-power, 10-W averagepower, spectrally narrow, diffraction-limited pulses from a photonic-crystal fiber amplifier," Opt. Express 13(22), 8999-9002 (2005).
[49] F. D. Teodoro and C. D. Brooks, "1.1 MW peak-power, 7 W average-power, high-spectral-brightness, diffraction-limited pulses from a photonic crystal fiber amplifier," Opt. Lett. 30(20), 2694-2696 (2005).
[50] R.M. Percival, D. Szebesta, C.P. Seltzer, S.D. Perrin, S.T. Davey, and M. Louka, "A 1.6-μm pumped 1.9-μm thulium-doped fluoride fiber laser and amplifier of very high efficiency," IEEE J. Quantum Electron., vol. 31, no. 3, pp. 489-493 (1995).
[51] R. C. Sharp, D. E. Spock, N. Pan, and J. Elliot, "190-fs passively mode-locked thulium fiber laser with a low threshold," Opt. Lett., vol. 21, no. 12, pp. 881-883 (1996).
[52] M. Jiang and P. Tayebati, "Stable 10 ns, kilowatt peak-power pulse generation from a gain-switched Tm-doped fiber laser," Opt. Lett., vol. 32, no. 13, pp. 1797-1799 (2007).
[53] Yulong Tang, F. Li, and J.Q. Xu, "High Peak-Power Gain-Switched Tm3+-doped Fiber Laser," IEEE Photon. Tech. Letts. 23, 893-895 (2011).
[54] S.D. Jackson and T.A. King, "Theoretical modeling of Tm-doped silica fiber lasers," J. Lightwave Technol., vol. 17, no. 5, pp. 948-956 (1999).
[55] Ashraf F. El-Sherif, Terence A. King, "Dynamics and self-pulsing effects in Tm3+-doped silica fibre lasers," Opt. Commun. 208, 381-389(2002).
[56] F.Z. Qamar and T.A. King, "Self-induced pulsations, Q-witching and mode-locking in Tm-silica fibre lasers", J. Mod. Opt. 52 (7), 1031-1043 (2005).

[57] D. Marcuse, "Pulsing behavior of a three-level laser with saturable absorber," IEEE J. Quantum Electron. 29, 2390–2396 (1993).
[58] S. D. Jackson and T. A. King, "Dynamics of the output of heavily Tm-doped double-clad silica fiber lasers," J. Opt. Soc. Am. B 16, 2178–2188 (1999).
[59] F. Z. Qamar and T. A. King, "Self-mode-locking effects in heavily doped single-clad Tm3+-doped silica fibre lasers," J. Mod. Opt. 52, 1053–1063 (2005).
[60] S. D. Jackson and T. A. King, "High-power diode-cladding pumped Tm-doped silica fiber laser," Opt. Lett. 23, 1462–1464 (1998).
[61] Y. Tang and J. Xu, "Self-induced pulsing in Tm3+-doped fiber lasers with different output couplings," Proc. SPIE 7276, 72760L–72760L-10 (2008).
[62] Michel J. F. Digonnet, "Rare-Earth-Doped Fiber Lasers and Amplifiers," P382, second ed. Marcel Dekker Inc., New York, Basel (2001).
[63] Yulong Tang, Jianqiu Xu, "Effects of Excited-state Absorption on Self-pulsing in Tm3+-doped Fiber Lasers," J. Opt. Soc. Am. B 27, 179-186 (2010).
[64] W. Koechner, "Solid-State Laser Engineering", Fifth Edition, springer-Verlag Berlin Heidelberg New York, pp.17–27, 1999.
[65] Gunnar Rustad and Knut Stenersen, "Modeling of Laser-Pumped Tm and Ho Lasers Accounting for Upconversion and Ground-State Depletion", IEEE Journal of Quantum Electronics, vol. 32, no. 9, pp. 1645–1656, September 1996.
[66] Igor Razdobreev and Alexander Shestakov, "Self-pulsing of a monolithic Tm-doped YAlO3 microlaser", Physical Review A, vol. 73, no. 5, pp. 053815 (1-5), 2006.
[67] S.D. Jackson and T.A. King, "Theoretical modeling of Tm-doped silica fiber lasers," J. Lightwave Tech. vol. 17, no. 5, 948-956, 1999.
[68] B. M. Walsh, N. P. Barnes, "Comparison of Tm:ZBLAN and Tm: silica fiber lasers; Spectroscopy and tunable pulsed laser operation around 1.9 μm," Appl. Phys. B, vol. 78, 325-333 (2004).
[69] Yulong Tang, Jianqiu Xu, "Model and characteristics of self-pulsing in Tm3+-doped silica fiber lasers," IEEE J. Quantum Electron. 47, 165-171 (2011).

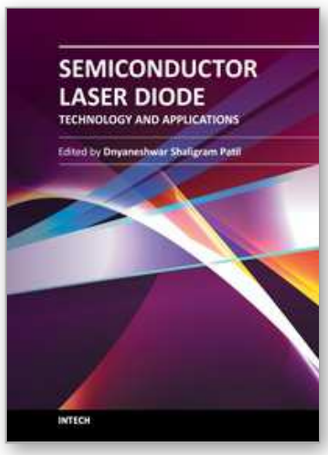

Semiconductor Laser Diode Technology and Applications
Edited by Dr. Dnyaneshwar Shaligram Patil

ISBN 978-953-51-0549-7
Hard cover, 376 pages
Publisher InTech
Published online 25, April, 2012
Published in print edition April, 2012

This book represents a unique collection of the latest developments in the rapidly developing world of semiconductor laser diode technology and applications. An international group of distinguished contributors have covered particular aspects and the book includes optimization of semiconductor laser diode parameters for fascinating applications. This collection of chapters will be of considerable interest to engineers, scientists, technologists and physicists working in research and development in the field of semiconductor laser diode, as well as to young researchers who are at the beginning of their career.

INTECH
open science | open minds

InTech Europe
University Campus STeP Ri
Slavka Krautzeka 83/A
51000 Rijeka, Croatia
Phone: +385 (51) 770 447
Fax: +385 (51) 686 166
www.intechopen.com

InTech China
Unit 405, Office Block, Hotel Equatorial Shanghai
No.65, Yan An Road (West), Shanghai, 200040, China
中国上海市延安西路65号上海国际贵都大饭店办公楼405单元
Phone: +86-21-62489820
Fax: +86-21-62489821

IntechOpen